JOC*Article*

Determination of the Absolute Configurations of Natural Products via Density Functional Theory Calculations of Vibrational Circular Dichroism, Electronic Circular Dichroism, and Optical Rotation: The Iridoids Plumericin and Isoplumericin

P. J. Stephens,* J. J. Pan, and F. J. Devlin

Department of Chemistry, University of Southern California, Los Angeles, California 90089-0482

K. Krohn

Department of Chemistry, University of Paderborn, Warburger Strasse 100, D-33098 Paderborn, Germany

T. Kurtán

Department of Organic Chemistry, University of Debrecen, P.O. Box 20, H-4010 Debrecen, Hungary

pstephen@usc.edu

Received January 25, 2007

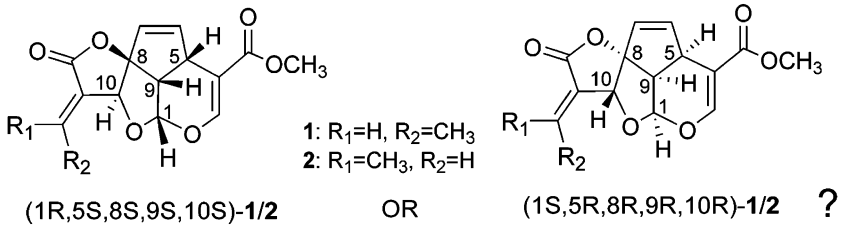

The absolute configurations (ACs) of the iridoid natural products, plumericin (**1**) and isoplumericin (**2**), have been re-investigated using vibrational circular dichroism (VCD) spectroscopy, electronic circular dichroism (ECD) spectroscopy, and optical rotatory dispersion (ORD). Comparison of DFT calculations of the VCD spectra of **1** and **2** to the experimental VCD spectra of the natural products, (+)-**1** and (+)-**2**, leads unambiguously to the AC (1*R*,5*S*,8*S*,9*S*,10*S*)-(+) for both **1** and **2**. In contrast, comparison of time-dependent DFT (TDDFT) calculations of the ECD spectra of **1** and **2** to the experimental spectra of (+)-**1** and (+)-**2** does not permit definitive assignment of their ACs. On the other hand, TDDFT calculations of the ORD of (1*R*,5*S*,8*S*,9*S*,10*S*)-**1** and -**2** over the range of 365−589 nm are in excellent agreement with the experimental data of (+)-**1** and (+)-**2**, confirming the ACs derived from the VCD spectra. Thus, the ACs initially proposed by Albers-Schönberg and Schmid are shown to be correct, and the opposite ACs recently derived from the ECD spectra of **1** and **2** by Elsässer et al. are shown to be incorrect. As a result, the ACs of other iridoid natural products obtained by chemical correlation with **1** and **2** are not in need of revision.

Introduction

The iridoid natural product, plumericin, one of the more than 200 iridoids to date found to occur in nature,[1] was first isolated from the roots of the plant *Plumeria multiflora* by Little and Johnstone in 1951[2] and was shown to exhibit anti-fungal and anti-bacterial activity. In 1960−1961, Albers-Schönberg and Schmid[3] isolated plumericin and its isomer, isoplumericin, from the roots of *Plumeria rubra var. alba* and, on the basis of chemical and spectroscopic studies, assigned their structures as **1** and **2**:

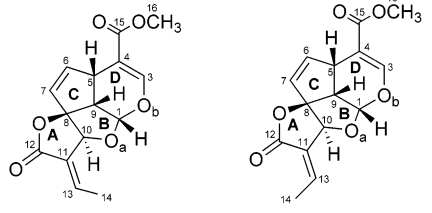

(1) (a) Bianco, A. The Chemistry of Iridoids. In *Studies in Natural Products Chemistry: Structure and Chemistry, Part A*; Atta-ur-Rahman, Ed.; Elsevier: Amsterdam, The Netherlands, 1990; Vol. 7, pp 439−497. (b) Bianco, A. *Pure Appl. Chem.* **1994**, *66*, 2335−2338. (c) AlHazimi, H. M. G.; Alkhathlan, H. Z. *J. Chem. Soc. Pakistan* **1996**, *18*, 336−357. (d) Franzyk, H. In *Progress in the Chemistry of Organic Natural Products*; Herz, W., Falk, H., Kirby, G. W., Moore, R. E., Eds.: Springer: Berlin, 2000; pp 1−114.

(2) Little, J. E.; Johnstone, D. B. *Arch. Biochem.* **1951**, *30*, 445−452.

10.1021/jo070155q CCC: $37.00
Published on Web 03/28/2007

TABLE 1. Calculated Relative Energies (Δ*E*)[a] and Free Energies (Δ*G*)[a] of the Conformations of 1

	MMFF94	B3LYP/6-31G*			B3LYP/TZ2P			B3PW91/TZ2P		
conformer	Δ*E*	Δ*E*	Δ*G*	*P* (%)[b]	Δ*E*	Δ*G*	*P* (%)[b]	Δ*E*	Δ*G*	*P* (%)[b]
1a	0.00	0.00	0.00	59.26	0.00	0.00	70.68	0.00	0.00	68.89
1b	0.49	0.35	0.39	30.67	0.64	0.63	24.41	0.59	0.59	25.63
1c	1.07	0.94	1.22	7.55	1.56	1.69	4.06	1.44	1.62	4.44
1d	1.80	1.55	1.87	2.52	2.46	2.61	0.85	2.82	2.48	1.04

[a] In kcal/mol. [b] Population percentages based on Δ*G*, assuming Boltzmann statistics at $T = 298.15$ K.

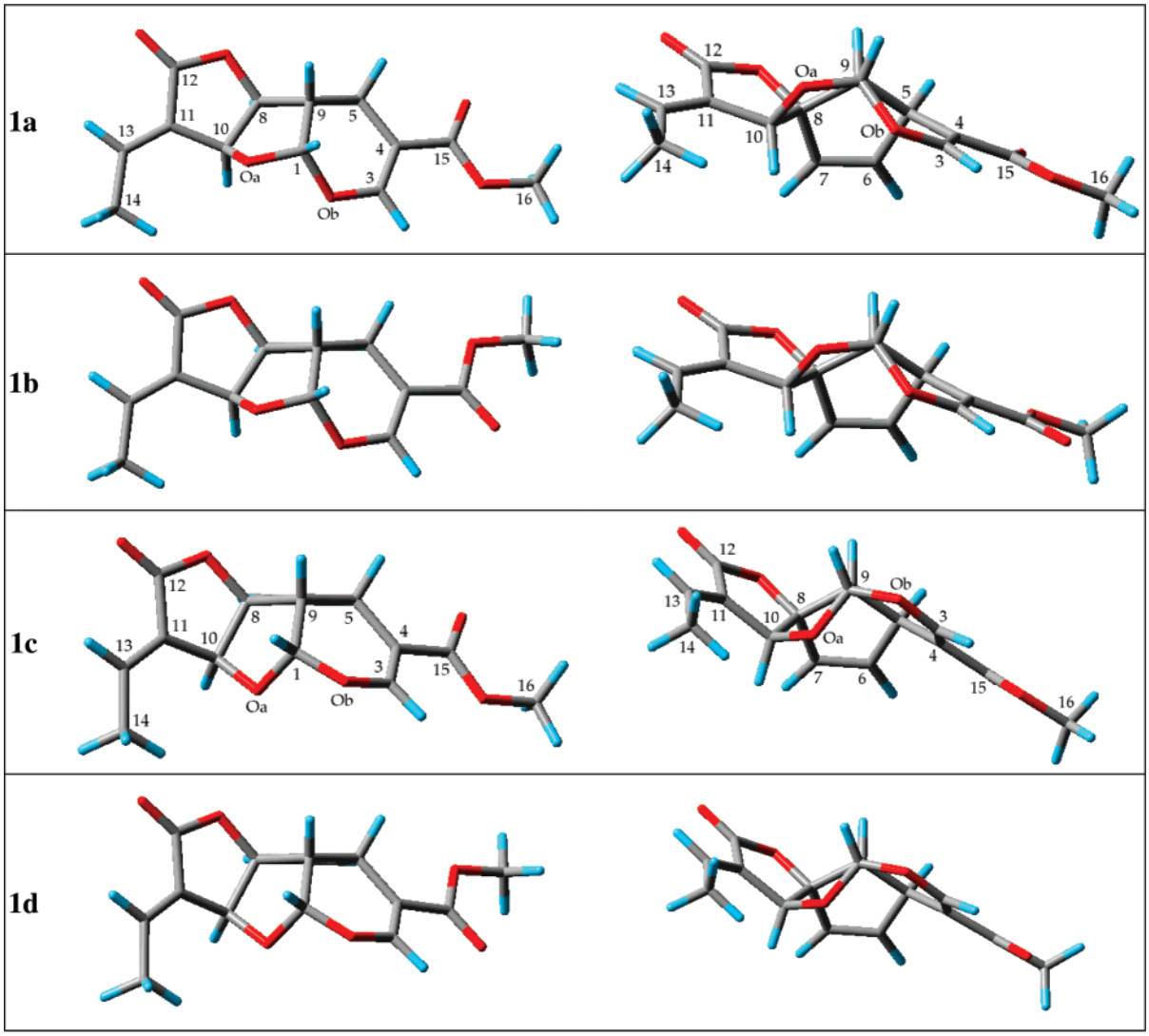

FIGURE 1. The B3PW91/TZ2P conformations of (1*R*,5*S*,8*S*,9*S*,10*S*)-**1**. The structures on the left are viewed with the plane of ring C horizontal, and C9 pointing toward the viewer. The structures on the right are viewed along the C1−C9 bond with C1 pointing toward the viewer.

Subsequently, **1** and **2** have been isolated from a variety of plants of the genus *Plumeria*[4] and also of the genera *Allamanda*,[5] *Nerium*,[6] *Himatanthus*,[7] and *Duroia*.[8] Total synthesis of (±)-**1** has been reported by Trost and co-workers[9] and by Parkes and Pattenden,[10] but to date, syntheses of optically active **1** and **2** have not been reported.

Very recently, the structures of **1** and **2** were re-evaluated by Elsässer et al.,[11] on the basis of X-ray crystal structure determinations and semiempirical quantum-mechanical calculations of their electronic circular dichroism (ECD) spectra. The X-ray structures confirmed the connectivities and relative configurations of **1** and **2** assigned by Albers-Schönberg and Schmid,[3] and subsequently generally accepted in the literature. However, the comparison of ECD spectra calculated using the DZDO program[12] and experimental ECD spectra led to the

(3) (a) Albers-Schönberg, G.; Schmid, H. *Chimia* **1960**, *14*, 127−128. (b) Albers-Schönberg, G.; Schmid, H. *Helv. Chim. Acta* **1961**, *44*, 1447−1473.

(4) (a) Kardono, L. B. S.; Tsauri, S.; Padmawinata, K.; Pezzuto, J. M.; Kinghorn, A. D. *J. Nat. Prod.* **1990**, *53*, 1447−1455. (b) Hamburger, M. O.; Cordell, G. A.; Ruangrungsi, N. *J. Ethnopharm.* **1991**, *33*, 289−292. (c) Dobhal, M. P.; Hasan, A. M.; Sharma, M. C.; Joshi, B. C. *Phytochemistry* **1999**, *51*, 319−321.

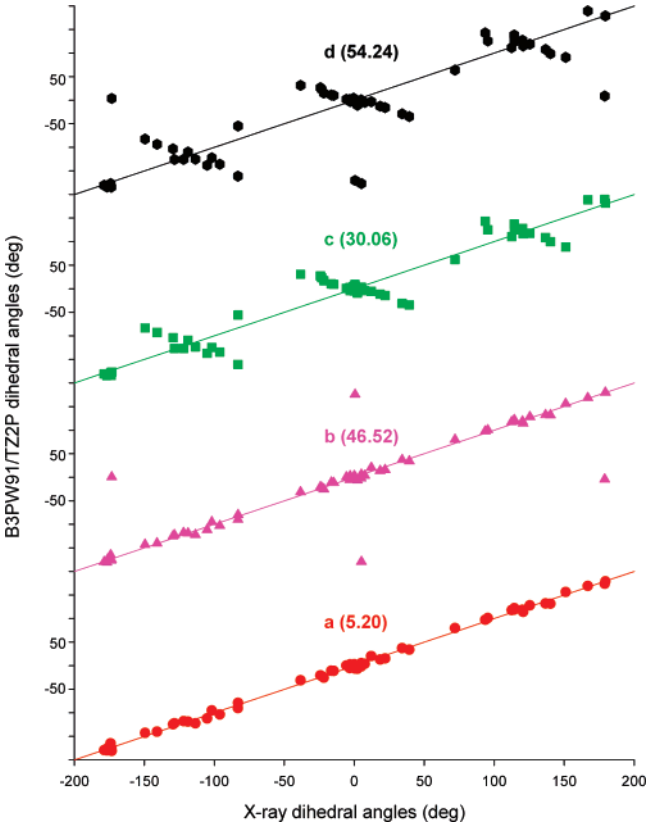

FIGURE 2. Comparison of dihedral angles of the X-ray structure of **1** and B3PW91/TZ2P calculated dihedral angles for the conformations **a**−**d** of **1**. The numbers in parentheses are the rms deviations between the calculated and X-ray dihedral angles.

conclusion that, for both **1** and **2**, the absolute configurations (ACs) assigned by Albers-Schönberg and Schmid,[3] and subsequently generally accepted in the literature, were incorrect and should be replaced by the ACs of the enantiomeric structures.

Since the 1960s, ECD spectroscopy, coupled with sector rules such as the octant rule or semiempirical quantum-mechanical calculations, has been the dominant chiroptical spectroscopic methodology used in determining ACs.[13] However, over the last decade, dramatic advances in chiroptical spectroscopy have occurred, leading to new and more reliable methods for determining ACs. The technique of vibrational circular dichroism (VCD) spectroscopy[14] has become more widely accessible, adding an additional experimental method to the classical methods of optical rotatory dispersion (ORD)[15] and ECD.[13] Most importantly, new theoretical methods for the calculation of chiroptical spectra based on ab initio density functional theory (DFT) have been developed and implemented, permitting much more reliable analyses of chiroptical spectra than previously possible. The application of DFT to the calculation of VCD spectra began in the early 1990s[16] and culminated in the fully-DFT-based implementation of Stephens' equation for vibrational rotational strengths[17] by Cheeseman et al.[18] This methodology was incorporated in the widely distributed program GAUSSIAN[19] in 1998. Since the first determinations of ACs based on comparisons of experimental VCD spectra to VCD spectra calculated using DFT,[20] the application of VCD spectroscopy to the determination of ACs has expanded enormously.[21] Subsequent to the application of DFT to VCD spectroscopy, time-dependent DFT (TDDFT) methods for the calculation of transparent spectral region optical rotations[22] and ECD spectra[23] have been developed, implemented, and tested. Increasing determination of ACs using either TDDFT calculations of OR or ECD, or both,[24] has resulted from these developments.

In a recent paper, we reported the concerted application of DFT calculations of VCD, OR, and ECD to the determination of the AC of the cytotoxic sesquiterpene natural product quadrone.[25] In this paper, we extend this work to the natural products **1** and **2**, with the goal of defining unambiguously their

(5) (a) Pai, B. R.; Subramaniam, P. S.; Rao, U. R. *Indian J. Chem.* **1970**, *8*, 851. (b) Kupchan, S. M.; Dessertine, A. L.; Blaylock, B. T.; Bryan, R. F. *J. Org. Chem.* **1974**, *39*, 2477−2482. (c) Yamauchi, T.; Abe, F.; Taki, M. *Chem. Pharm. Bull.* **1981**, *29*, 3051−3055. (d) Bhattacharyya, J.; Morais, M. S. Q. *J. Nat. Prod.* **1986**, *49*, 354−371. (e) Anderson, J. E.; Chang, C. J.; McLaughlin, J. L. *J. Nat. Prod.* **1988**, *51*, 307−308. (f) Vilegas, J. H. Y.; Hachich, E. M.; Garcia, M.; Brasileiro, A.; Carneiro, M. A. G.; Campos, V. L. B. *Rev. Latinoam. Quim.* **1992**, *22*, 44−45. (g) Vilegas, J. H. Y.; Hachich, E. M.; Garcia, M.; Basileiro, A.; Carneiro, M. A. G.; Campos, V. L. B. *Rev. Latinoam. Quim.* **1994**, *23*, 73−75. (h) Abdel-Kader, M. S.; Wisse, J.; Evans, R.; Werff, H.; Kingston, D. G. I. *J. Nat. Prod.* **1997**, *60*, 1294−1297.

(6) Basu, D.; Chatterjee, A. *Indian J. Chem.* **1973**, *11*, 297.

(7) (a) Vanderlei, M. F.; Silva, M. S.; Gottlieb, H. E.; Braz-Filho, R. *J. Braz. Chem. Soc.* **1991**, *2*, 51−55. (b) Vilegas, J. H. Y.; Hachich, E. M.; Garcia, M.; Brasileiro, A.; Carneiro, M. A. G.; Campos, V. L. B. *Rev. Latinoam. Quim.* **1992**, *22*, 44−45. (c) Vilegas, J. H. Y.; Hachich, E. M.; Garcia, M.; Basileiro, A.; Carneiro, M. A. G.; Campos, V. L. B. *Rev. Latinoam. Quim.* **1994**, *23*, 73−75. (d) Abdel-Kader, M. S.; Wisse, J.; Evans, R.; Werff, H.; Kingston, D. G. I. *J. Nat. Prod.* **1997**, *60*, 1294−1297. (e) Wood, C. A.; Lee, K.; Vaisberg, A. J.; Kingston, D. G. I.; Neto, C. C.; Hammond, G. B. *Chem. Pharm. Bull.* **2001**, *49*, 1477−1478.

(8) Page, J. E.; Madrinan, S.; Towers, G. H. N. *Experientia* **1994**, *50*, 840−842.

(9) (a) Trost, B. M.; Balkovec, J. M.; Mao, M. K. T. *J. Am. Chem. Soc.* **1983**, *105*, 6755−6757. (b) Trost, B. M.; Mao, M. K. T.; Balkovec, J. M.; Buhlmayer, P. *J. Am. Chem. Soc.* **1986**, *108*, 4965−4973. (c) Trost, B. M.; Balkovec, J. M.; Mao, M. K. T. *J. Am. Chem. Soc.* **1986**, *108*, 4974−4983.

(10) (a) Parks, K. E. B.; Pattenden, G. *Tetrahedron Lett.* **1986**, *27*, 1305−1308. (b) Parks, K. E. B.; Pattenden, G. *J. Chem. Soc., Perkin Trans. 1* **1988**, 1119−1134.

(11) Elsässer, B.; Krohn, K.; Akhtar, M. N.; Flörke, U.; Kouam, S. F.; Kuigoua, M. G.; Ngadjui, B. T.; Abegaz, B. M.; Antus, S.; Kurtán, T. *Chem. Biodiversity* **2005**, *2*, 799−808.

(12) Downing, J. W. *DZDO*, Department of Chemistry and Biochemistry, University of Colorado, Boulder, CO.

(13) (a) Lightner, D. A.; Gurst, J. E. *Organic Conformational Analysis and Stereochemistry from Circular Dichroism Spectroscopy*; John Wiley & Sons, Inc.: New York, 2000. (b) *Circular Dichroism: Principles and Applications*, 2nd ed.; Berova, N., Nakanishi, K., Woody, R. W., Eds.; John Wiley & Sons, Inc.: New York, 2000.

(14) (a) Stephens, P. J.; Clark, R. In *Optical Activity and Chiral Discrimination*; Mason, S. F., Ed.; Riedel: Dordrecht, The Netherlands, 1979; pp 263−287. (b) Stephens, P. J.; Lowe, M. A. *Annu. Rev. Phys. Chem.* **1985**, *36*, 213−241. (c) Stephens, P. J.; Devlin, F. J. *Chirality* **2000**, *12*, 172−179.

(15) Djerassi, C. *Optical Rotatory Dispersion*; McGraw-Hill Book Company, Inc.: New York, 1960.

(16) (a) Stephens, P. J.; Devlin, F. J.; Chabalowski, C. F.; Frisch, M. J. *J. Phys. Chem.* **1994**, *98*, 11623−11627. (b) Stephens, P. J.; Devlin, F. J.; Ashvar, C. S.; Chabalowski, C. F.; Frisch, M. J. *Faraday Discuss.* **1994**, *99*, 103−119. (c) Bak, K. L.; Devlin, F. J.; Ashvar, C. S.; Taylor, P. R.; Frisch, M. J.; Stephens, P. J. *J. Phys. Chem.* **1995**, *99*, 14918−14922. (d) Devlin, F. J.; Finley, J. W.; Stephens, P. J.; Frisch, M. J. *J. Phys. Chem.* **1995**, *99*, 16883−16902. (e) Stephens, P. J.; Devlin, F. J.; Ashvar, C. S.; Bak, K. L.; Taylor, P. R.; Frisch, M. J. In *Chemical Applications of Density-Functional Theory*; Laird, B.B., Ross, R. B., Ziegler, Z., Eds.; ACS Symposium Series 629; American Chemical Society: Washington, DC, 1996; pp 105−113.

(17) Stephens, P. J. *J. Phys. Chem.* **1985**, *89*, 748−752.

(18) Cheeseman, J. R.; Frisch, M. J.; Devlin, F. J.; Stephens, P. J. *Chem. Phys. Lett.* **1996**, *252*, 211−220.

(19) GAUSSIAN, Gaussian Inc., www.gaussian.com.

(20) See, for example: (a) Ashvar, C. S.; Stephens, P. J.; Eggimann, T.; Wieser, H. *Tetrahedron: Asymmetry* **1998**, *9*, 1107−1110. (b) Aamouche, A.; Devlin, F. J.; Stephens, P. J. *Chem. Commun.* **1999**, 361−362. (c) Stephens, P. J.; Devlin, F. J. *Chirality* **2000**, *12*, 172−179.

TABLE 2. Calculated Relative Energies (Δ*E*)[a] and Free Energies (Δ*G*)[a] of the Conformations of 2

	MMFF94	B3LYP/6-31G*			B3LYP/TZ2P			B3PW91/TZ2P		
conformer	Δ*E*	Δ*E*	Δ*G*	*P* (%)[b]	Δ*E*	Δ*G*	*P* (%)[b]	Δ*E*	Δ*G*	*P* (%)[b]
2a	0.00	0.00	0.00	64.23	0.00	0.00	75.36	0.00	0.00	73.06
2b	0.49	0.39	0.56	24.77	0.67	0.83	18.62	0.63	0.79	19.34
2c	0.72	1.18	1.19	8.62	1.68	1.60	5.05	1.51	1.45	6.35
2d	1.41	1.78	1.95	2.38	2.55	2.58	0.97	2.34	2.41	1.25

[a] In kcal/mol. [b] Population percentages based on Δ*G*, assuming Boltzmann statistics at $T = 298.15$ K.

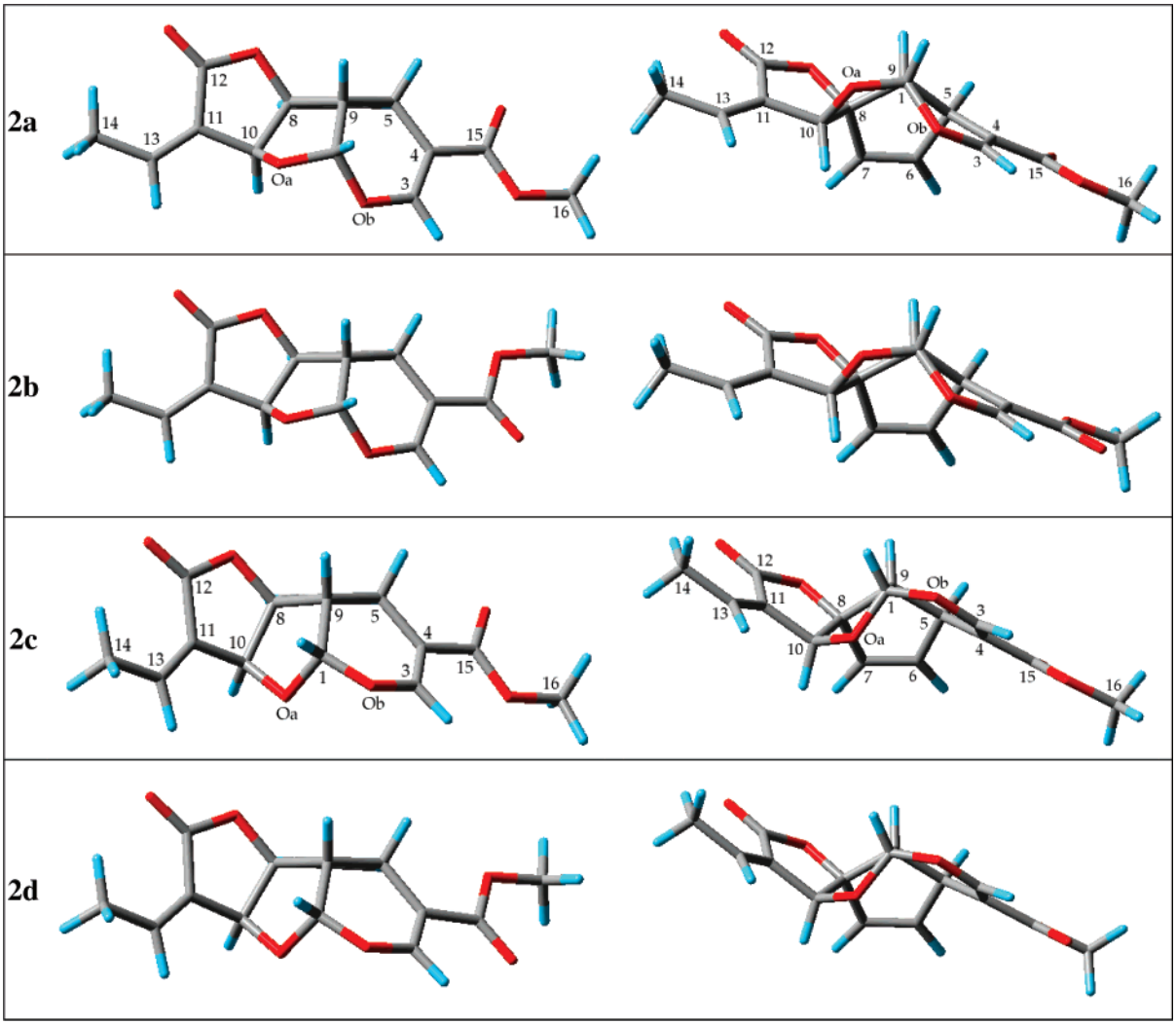

FIGURE 3. The B3PW91/TZ2P conformations of (1*R*,5*S*,8*S*,9*S*,10*S*)-**2**. The structures on the left are viewed with the plane of ring C horizontal, and C9 pointing toward the viewer. The structures on the right are viewed along the C1−C9 bond with C1 pointing toward the viewer.

ACs, which previously were used for the configurational assignment of related iridoids including allamcin,[4a] allamandicin,[5b] plumieride coumarate,[26] and their respective glucosides by chemical correlation.

Results

Isolation of Plumericin and Isoplumericin. The dextrorotatory natural products **1** and **2** were isolated from *Plumeria rubra* and purified as described previously.[11]

Conformational Analysis. A Monte Carlo search of the conformations of (1*R*,5*S*,8*S*,9*S*,10*S*)-**1** using the MMFF94 molecular mechanics force field identified four conformations, **a**−**d**, within a 10 kcal/mol window. The relative energies of these conformations are given in Table 1. Reoptimization of the structures of conformations **1a**−**1d** was then carried out using DFT at the B3LYP/6-31G*, B3LYP/TZ2P, and B3PW91/TZ2P levels, with the results given in Table 1. For each conformation at each level, harmonic vibrational frequencies were then calculated to confirm that all conformations are stable and also to permit the relative free energies of the four conformations to be calculated, with the results given in Table 1. Both MMFF94 and DFT calculations give energies in the order **1a** < **1b** < **1c** < **1d**; DFT calculations give free energies in the same order. Using Boltzmann statistics, equilibrium populations at room temperature of the four conformations can be calculated from the DFT relative free energies, with the

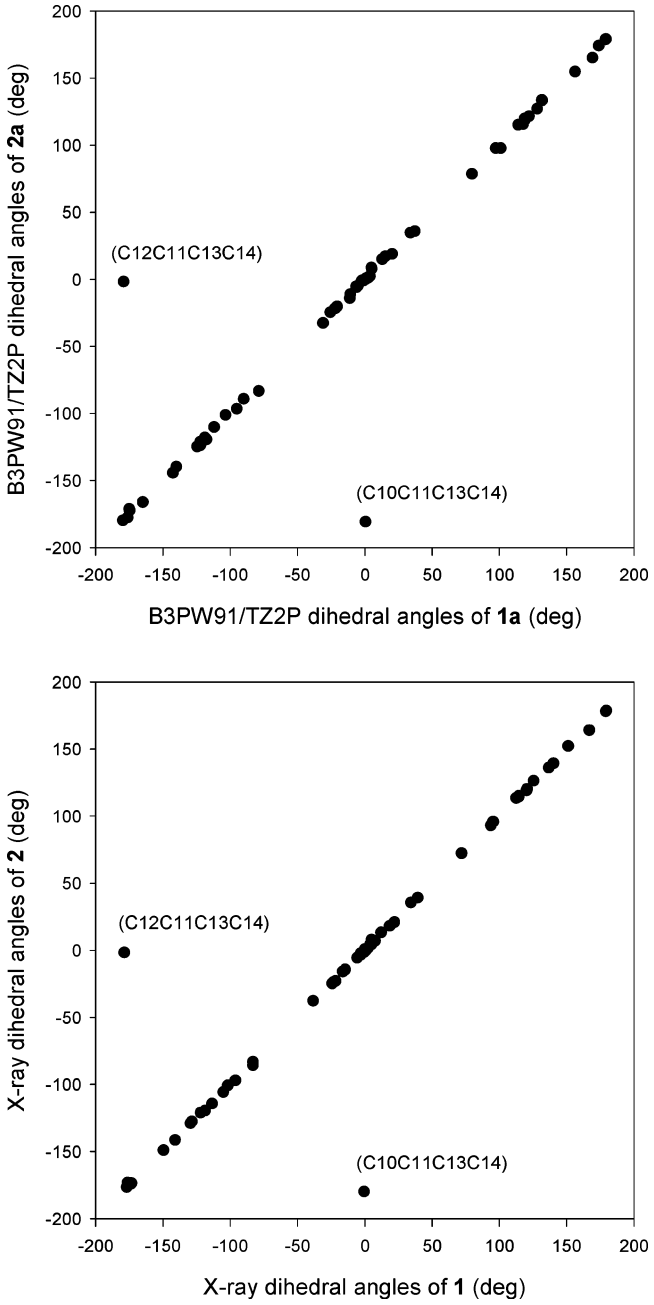

FIGURE 4. Comparison of B3PW91/TZ2P calculated dihedral angles for the conformations **1a** and **2a** (top), and dihedral angles for the X-ray structures of **1** and **2** (bottom).

results given in Table 1. At all levels, conformations **1a** and **1b** are predicted to constitute >∼90% of the equilibrium mixture, with **1c** and **1d** correspondingly <∼10%.

The structures of the conformations **1a**−**1d** are illustrated in Figure 1. The principal variations in structure are associated with the rings B and D and the methoxycarbonyl group substituent of ring D. In conformations **1a** and **1c**, the methoxycarbonyl group is oriented with the C═O group in the s-*trans* conformation with respect to the C3═C4 group, while **1b** and **1d** have the s-*cis* conformation. In conformations **1a** and **1b**, rings B and D have the same conformations, while in conformations **1c** and **1d**, the O atoms of these rings are oppositely puckered.

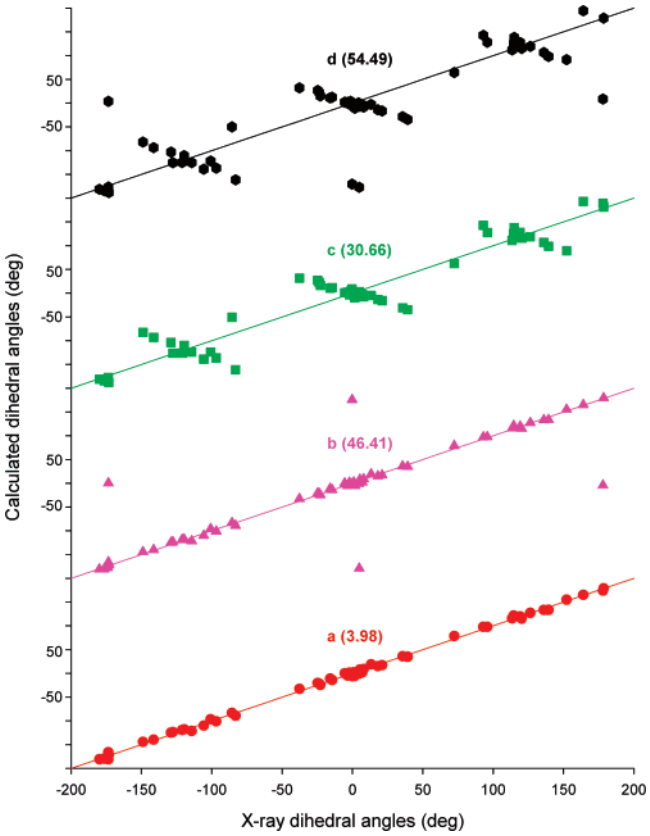

FIGURE 5. Comparison of dihedral angles of the X-ray structure of **2** and B3PW91/TZ2P calculated dihedral angles for the conformations **a**−**d** of **2**. The numbers in parentheses are the rms deviations between the calculated and X-ray dihedral angles.

In all conformations **1a**−**1d**, the methyl group and the carbonyl O of the methoxycarbonyl substituent of ring D are *cis*. A B3LYP/6-31G* potential energy surface (PES) scan with respect to the dihedral angle C4C15OC16 for **1a** shows (Figure S1 of the Supporting Information (SI)) that the *trans* conformation of the methoxycarbonyl group is >10 kcal/mol higher in energy than the *cis* conformation and, therefore, not significantly populated at room temperature.

(21) (a) Aamouche, A.; Devlin, F. J.; Stephens, P. J. *J. Am. Chem. Soc.* **2000**, *122*, 2346−2354. (b) Aamouche, A.; Devlin, F. J.; Stephens, P. J.; Drabowicz, J.; Bujnicki, B.; Mikolajczyk, M. *Chem.—Eur. J.* **2000**, *6*, 4479−4486. (c) Stephens, P. J.; Aamouche, A.; Devlin, F. J.; Superchi, S.; Donnoli, M. I.; Rosini, C. *J. Org. Chem.* **2001**, *66*, 3671−3677. (d) Devlin, F. J.; Stephens, P. J.; Scafato, P.; Superchi, S.; Rosini, C. *Tetrahedron: Asymmetry* **2001**, *12*, 1551−1558. (e) Stephens, P. J.; Devlin, F. J.; Aamouche, A. In *Chirality: Physical Chemistry*; Hicks, J. M., Ed.; ACS Symposium Series 810; American Chemical Society: Washington, DC, 2002; Chapter 2, pp 18−33. (f) Devlin, F. J.; Stephens, P. J.; Scafato, P.; Superchi, S.; Rosini, C. *Chirality* **2002**, *14*, 400−406. (g) Devlin, F. J.; Stephens, P. J.; Oesterle, C.; Wiberg, K. B.; Cheeseman, J. R.; Frisch, M. J. *J. Org. Chem.* **2002**, *67*, 8090−8096. (h) Stephens, P. J. In *Computational Medicinal Chemistry for Drug Discovery*; Bultinck, P., Winter, H., Langenaecker, W., Tollenaere, J., Eds.; Dekker: New York, 2003; Chapter 26, pp 699−725. (i) Cere, V.; Peri, F.; Pollicino, S.; Ricci, A.; Devlin, F. J.; Stephens, P. J.; Gasparrini, F.; Rompietti, R.; Villani, C. *J. Org. Chem.* **2005**, *70*, 664−669. (j) Stephens, P. J.; McCann, D. M.; Devlin, F. J.; Flood, T. C.; Butkus, E.; Stoncius, S.; Cheeseman, J. R. *J. Org. Chem.* **2005**, *70*, 3903−3913. (k) Devlin, F. J.; Stephens, P. J.; Besse, P. *Tetrahedron: Asymmetry* **2005**, *16*, 1557−1566. (l) Devlin, F. J.; Stephens, P. J.; Bortolini, O. *Tetrahedron: Asymmetry* **2005**, *16*, 2653−2663. (m) Carosati, E.; Cruciani, G.; Chiarini, A.; Budriesi, R.; Ioan, P.; Spisani, R.; Spinelli, D.; Cosimelli, B.; Fusi, F.; Frosini, M.; Matucci, R.; Gasparrini, F.; Ciogli, A.; Stephens, P. J.; Devlin, F. J. *J. Med. Chem.* **2006**, *49*, 5206−5216.

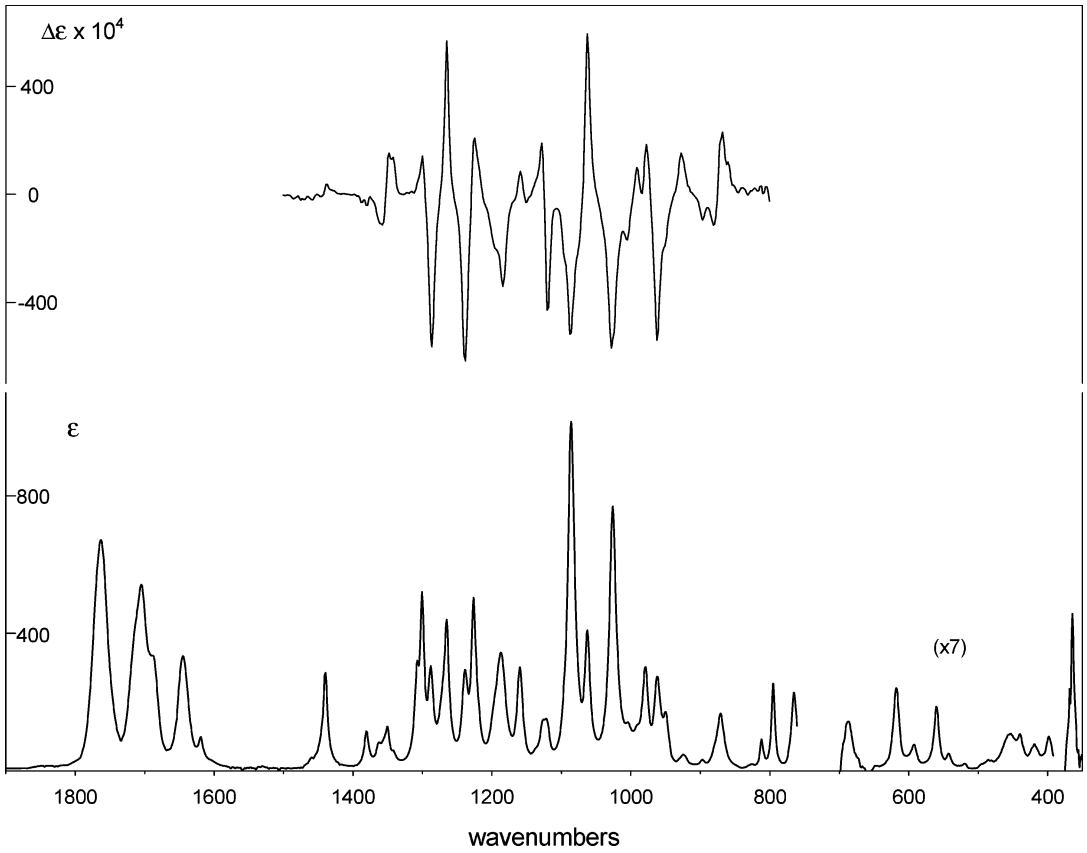

FIGURE 6. Experimental IR and VCD spectra of (+)-**1**. The IR spectrum was measured in $CDCl_3$ solution (0.069 M) for the ranges (pathlengths) of 662−700 cm^{-1} (109 μm), 761−770 cm^{-1} (109 μm), 770−883 cm^{-1} (239 μm), and 943−1900 cm^{-1} (239 μm) and in $CHCl_3$ solution (0.069 M) for the ranges (pathlengths) of 350−375 cm^{-1} (239 μm), 391−654 cm^{-1} (597 μm), and 879−942 cm^{-1} (597 μm). The VCD spectrum was measured in $CDCl_3$ solution (0.069 M) for the ranges (pathlengths) of 800−840 cm^{-1} (597 μm), 840−875 cm^{-1} (239 μm), 963−1067 cm^{-1} (239 μm), 1067−1100 cm^{-1} (109 μm), 1100−1326 cm^{-1} (239 μm), and 1326−1500 cm^{-1} (597 μm) and in $CHCl_3$ solution (0.069 M) for the ranges (pathlengths) of 875−917 cm^{-1} (597 μm), 917−934 cm^{-1} (239 μm), and 934−963 cm^{-1} (597 μm).

The structure of **1** determined using X-ray crystallography has been reported by Elsässer et al.[11] The calculated structures of conformations **1a**−**1d** have been compared to the X-ray structure, using the "heavy-atom" dihedral angles listed in Table S1 of the SI. Plots of calculated dihedral angles versus experimental dihedral angles, shown in Figure 2 and Figure S1 of the SI, demonstrate clearly that, at all levels of calculation, the calculated structures of conformation **1a** are in the best agreement with experiment. This both supports the reliability of our calculated conformational structures and shows that the conformation of **1** in the crystalline solid state is that of the lowest energy conformation (which, of course, is not universally the case).

Conformational analysis of (1*R*,5*S*,8*S*,9*S*,10*S*)-**2** was carried out identically to that of **1** with the results given in Table 2 and Table S2 of the SI, and Figures 3−5 and Figure S2 of the SI. As can be seen in Figure 3, conformations **2a**−**2d** of **2** are qualitatively identical in structure to the conformations **1a**−**1d** of **1**, except for the orientation of the C14 methyl group. Their energies and free energies are ordered identically (Table 2). Again, room-temperature equilibrium populations, based on DFT relative free energies, are >∼90% for **2a** and **2b** and <∼10% for **2c** and **2d** (Table 2). Dihedral angles of **2a**−**2d** are listed in Table S2 of the SI. B3PW91/TZ2P dihedral angles of **2a** are compared to the corresponding dihedral angles of **1a** in Figure 4; not surprisingly, with the exception of the dihedral angles C10C11C13C14 and C12C11C13C14, the predicted dihedral angles for **1a** and **2a** are extremely similar. The MMFF94, B3LYP/6-31G*, B3LYP/TZ2P, and B3PW91/TZ2P dihedral angles of **2a**−**2d** are compared to the dihedral angles determined

(22) (a) Stephens, P. J.; Devlin, F. J.; Cheeseman, J. R.; Frisch, M. J.; Mennucci, B.; Tomasi, J. *Tetrahedron: Asymmetry* **2000**, *11*, 2443−2448. (b) Stephens, P. J.; Devlin, F. J.; Cheeseman, J. R.; Frisch, M. J. *J. Phys. Chem. A* **2001**, *105*, 5356−5371. (c) Stephens, P. J.; Devlin, F. J.; Cheeseman, J. R.; Frisch, M. J. *Chirality* **2002**, *14*, 288−296. (d) Mennucci, B.; Tomasi, J.; Cammi, R.; Cheeseman, J. R.; Frisch, M. J.; Devlin, F. J.; Gabriel, S.; Stephens, P. J. *J. Phys. Chem. A* **2002**, *106*, 6102−6113. (e) McCann, D. M.; Stephens, P. J.; Cheeseman, J. R. *J. Org. Chem.* **2004**, *69*, 8709−8717. (f) Stephens, P. J.; McCann, D. M.; Cheeseman, J. R.; Frisch, M. J. *Chirality* **2005**, *17*, S52−S64.

(23) (a) Stephens, P. J.; McCann, D. M.; Butkus, E.; Stoncius, S.; Cheeseman, J. R.; Frisch, M. J. *J. Org. Chem.* **2004**, *69*, 1948−1958. (b) McCann, D. M.; Stephens, P. J. *J. Org. Chem.* **2006**, *71*, 6074−6098.

(24) (a) Stephens, P. J.; Devlin, F. J.; Cheeseman, J. R.; Frisch, M. J. *Chirality* **2002**, *14*, 288−296. (b) Stephens, P. J.; Devlin, F. J.; Cheeseman, J. R.; Frisch, M. J.; Rosini, C. *Org. Lett.* **2002**, *4*, 4595−4598. (c) Stephens, P. J.; Devlin, F. J.; Cheeseman, J. R.; Frisch, M. J.; Bortolini, O.; Besse, P. *Chirality* **2003**, *15*, S57−S64. (d) McCann, D. M.; Stephens, P. J.; Cheeseman, J. R. *J. Org. Chem.* **2004**, *69*, 8709−8717. (e) Stephens, P. J.; McCann, D. M.; Butkus, E.; Stoncius, S.; Cheeseman, J. R.; Frisch, M. J. *J. Org. Chem.* **2004**, *69*, 1948−1958. (f) Stephens, P. J.; McCann, D. M.; Devlin, F. J.; Cheeseman, J. R.; Frisch, M. J. *J. Am. Chem. Soc.* **2004**, *126*, 7514−7521. (g) McCann, D. M.; Stephens, P. J. *J. Org. Chem.* **2006**, *71*, 6074−6098.

(25) Stephens, P. J.; McCann, D. M.; Devlin, F. J.; Smith, A. B., III. *J. Nat. Prod.* **2006**, *69*, 1055−1064.

(26) Coppen, J. J. W. *Phytochemistry* **1983**, *22*, 179−182.

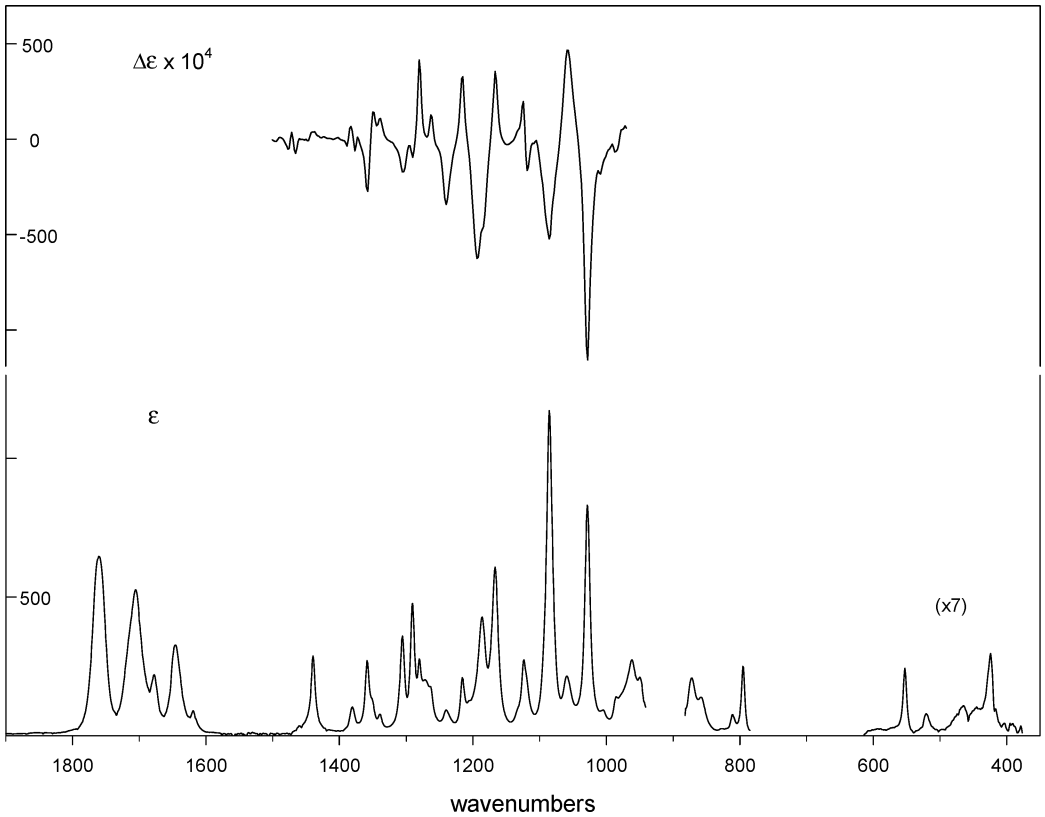

FIGURE 7. Experimental IR and VCD spectra of (+)-**2**. The IR spectrum was measured in $CDCl_3$ solution (0.031 M) for the ranges (pathlengths) of 377−614 cm^{-1} (597 μm), 785−880 cm^{-1} (239 μm), and 941−1900 cm^{-1} (597 μm). The VCD spectrum was measured in $CDCl_3$ solution (0.031 M) for the ranges (pathlengths) of 970−991 cm^{-1} (597 μm), 991−1041 cm^{-1} (239 μm), 1041−1070 cm^{-1} (597 μm), 1070−1103 cm^{-1} (239 μm), and 1103−1500 cm^{-1} (597 μm).

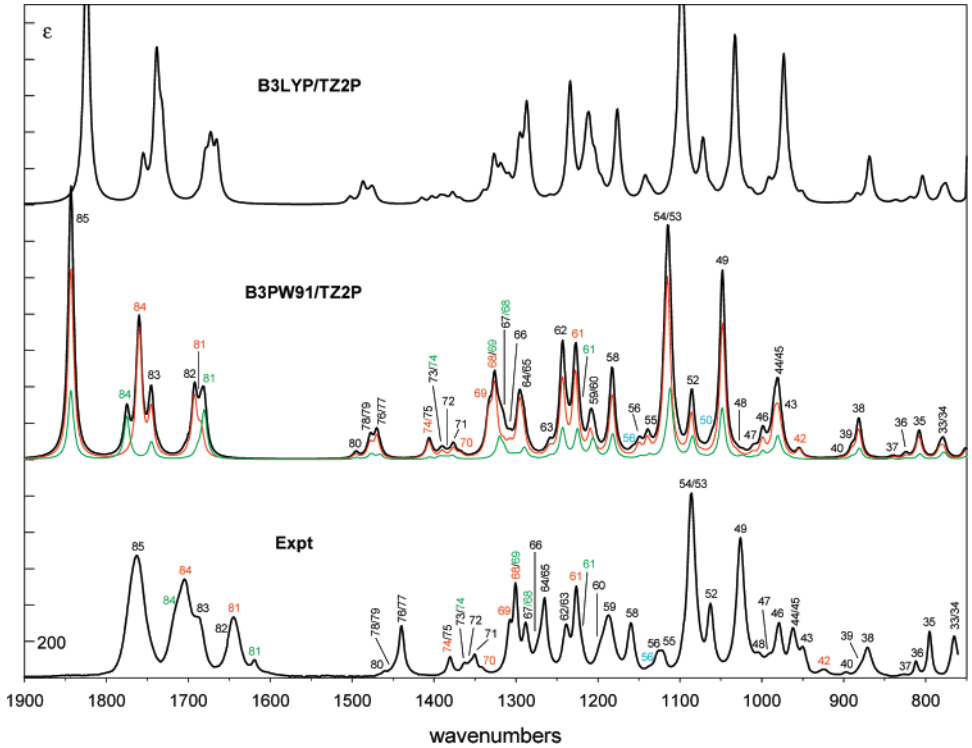

FIGURE 8. Comparison of the experimental and B3LYP/TZ2P and B3PW91/TZ2P IR spectra of **1** for the range of 750−1900 cm^{-1}. The black calculated spectra are conformationally averaged. The red and green calculated spectra are the population-weighted IR spectra of **1a** and **1b**, respectively. The numbers define the fundamentals contributing to resolved bands. Red, green, and cyan numbers refer to fundamentals of **1a**, **1b**, and **1c**/**1d**, respectively. Black numbers are used when the bands of **1a** and **1b** are not resolved. Bandshapes of the calculated spectra are Lorentzian ($\gamma = 4.0$ cm^{-1}). The assignment of the experimental spectrum is based on the B3PW91/TZ2P calculated spectrum.

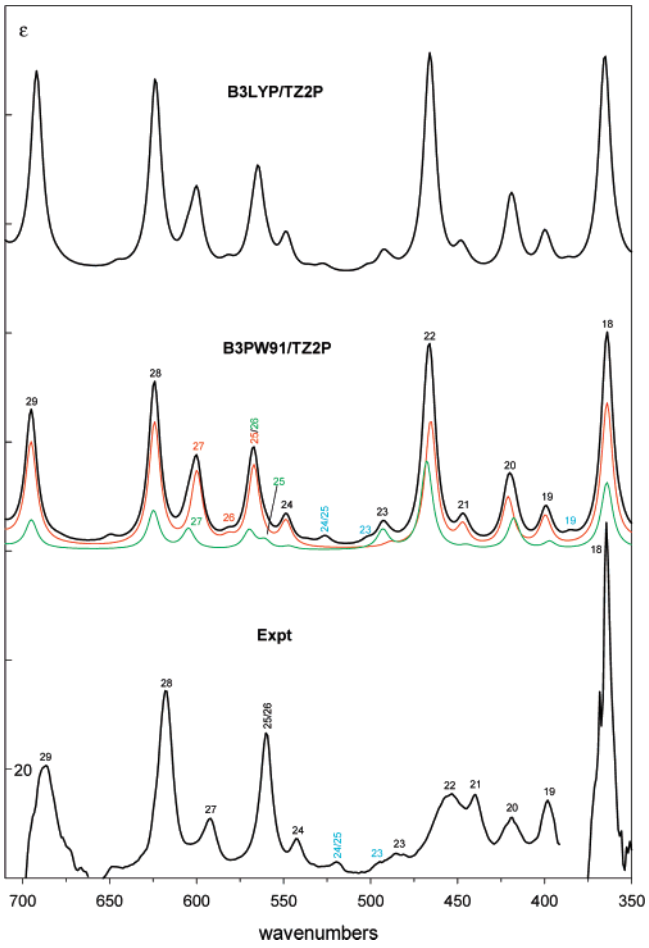

FIGURE 9. Comparison of the experimental and B3LYP/TZ2P and B3PW91/TZ2P IR spectra of **1** for the range of 350−700 cm^{-1}. The black calculated spectra are conformationally averaged. The red and green calculated spectra are the population-weighted IR spectra of **1a** and **1b**, respectively. The numbers define the fundamentals contributing to resolved bands. Red, green, and cyan numbers refer to fundamentals of **1a**, **1b**, and **1c**/**1d**, respectively. Black numbers are used when the bands of **1a** and **1b** are not resolved. Bandshapes of the calculated spectra are Lorentzian (γ = 4.0 cm^{-1}). The assignment of the experimental spectrum is based on the B3PW91/TZ2P calculated spectrum.

via X-ray crystallography of **2**[11] in Figure 5 and Figure S2 of the SI. As with **1**, the comparison clearly shows that the conformation of **2** in the crystalline solid state is that of the lowest energy conformation, **2a**. Dihedral angles of both crystal structures **1** and **2** are compared in Figure 4; except for the dihedral angles C10C11C13C14 and C12C11C13C14, the experimental dihedral angles of **1** and **2** are extremely similar, consistent with the DFT predictions for conformations **1a** and **2a**.

IR and VCD Spectra. The IR and VCD spectra of 0.069 M $CHCl_3$ and $CDCl_3$ solutions of (+)-**1** have been measured using cells of pathlengths 109, 239, and 597 μm; the spectra obtained are shown in Figure 6 for the range of 350−1900 cm^{-1}. With the exception of the 700−760 cm^{-1} region, where both $CHCl_3$ and $CDCl_3$ absorb, by combining spectra in both solvents at all three pathlengths, the IR spectrum of **1** over this spectral range is obtained. The lower frequency limit of the chiral IR VCD spectrometer is ∼800 cm^{-1}. While VCD spectra can be measured up to 2000 cm^{-1}, despite the use of the dual PEM accessory, artifact levels are much larger in the carbonyl stretching region (1600−1900 cm^{-1}), and as a result, reliable VCD spectra can only be obtained when both enantiomers of the molecule (or one enantiomer together with the racemate) are available, permitting artifacts to be subtracted.[20,21] In this region, VCD spectra obtained from single enantiomers are not reliable, as illustrated by the spectra obtained for (+)-**1**, using two different PEM center frequency settings (1200 and 1800 cm^{-1}), in Figure S3 of the SI. The IR and VCD spectra of **2** were only measured in $CDCl_3$ solution. The spectra of a 0.031 M $CDCl_3$ solution of (+)-**2** over the range of 375−1900 cm^{-1} are shown in Figure 7.

The harmonic vibrational frequencies and dipole strengths of (1*R*,5*S*,8*S*,9*S*,10*S*)-**1** and (1*R*,5*S*,8*S*,9*S*,10*S*)-**2** have been calculated at the B3LYP/TZ2P and B3PW91/TZ2P levels for conformations **a**−**d**, with the results given in Tables S3 and S4 of the SI. The IR spectra obtained thence using Lorentzian bandshapes are shown in Figures S4−7 of the SI, together with the spectra weighted by the room-temperature equilibrium populations and their sum, the conformationally averaged IR spectrum. While for both **1** and **2** there is considerable similarity between the IR spectra of the four conformations, they are not identical. As a result, for each molecule, the conformationally averaged spectrum is more complex than the spectra of the individual conformations. However, the complexity is diminished by the smallness of the populations of conformations **c** (<7%) and **d** (<2%). To a good approximation, the conformationally averaged spectra are due to conformations **a** and **b** only. The B3LYP/TZ2P and B3PW91/TZ2P conformationally averaged IR spectra of **1** and **2** are compared to each other and to the experimental IR spectra in Figures 8−11. While the spectra given by the two functionals are similar, they are not identical, especially over the range of 1100−1500 cm^{-1}. For both **1** and **2**, the B3PW91/TZ2P spectra are in better agreement with experiment. As a result, they are the basis for the assignments of the experimental spectra detailed in Figures 8−11 and Tables S3 and S4 of the SI. For **1**, a number of bands observed experimentally can be assigned to the modes of individual conformations: modes 42, 61, 69, 70, 81, and 84 of **1a** are resolved, as are modes 81 and 84 of **1b** and modes 23−25 and 56 of **1c**/**1d**. Likewise, for **2**, modes 20, 21, 23, 24, 26, 42, 66, 68, 82, and 84 of **2a** are resolved, as are modes 20, 21, 23, 24, 68, and 84 of **2b** and mode 56 of **2c**/**2d**. The excellent agreement of the calculated and experimental IR spectra of **1** and **2** and the observation of bands of individual conformations strongly support the reliability of the B3PW91/TZ2P DFT conformational analyses of **1** and **2** and the IR spectra of their conformations. Experimental frequencies and dipole strengths have been obtained from the experimental IR spectra via Lorentzian fitting with the results given in Figures S8 and S9 of the SI and Tables S3 and S4 of the SI. Calculated and experimental frequencies and dipole strengths, the latter conformationally averaged where unresolved, are compared in Figures 12−15.

The harmonic rotational strengths of (1*R*,5*S*,8*S*,9*S*,10*S*)-**1** and (1*R*,5*S*,8*S*,9*S*,10*S*)-**2** have been calculated at the B3LYP/TZ2P and B3PW91/TZ2P levels for conformations **a**−**d**, with the results given in Tables S3 and S4 of the SI. The VCD spectra obtained thence using Lorentzian bandshapes are shown in Figures S10−13 of the SI, together with the spectra weighted by the room-temperature equilibrium populations and their sums, the conformationally averaged VCD spectra. As has been the case for all conformationally flexible molecules studied previ-

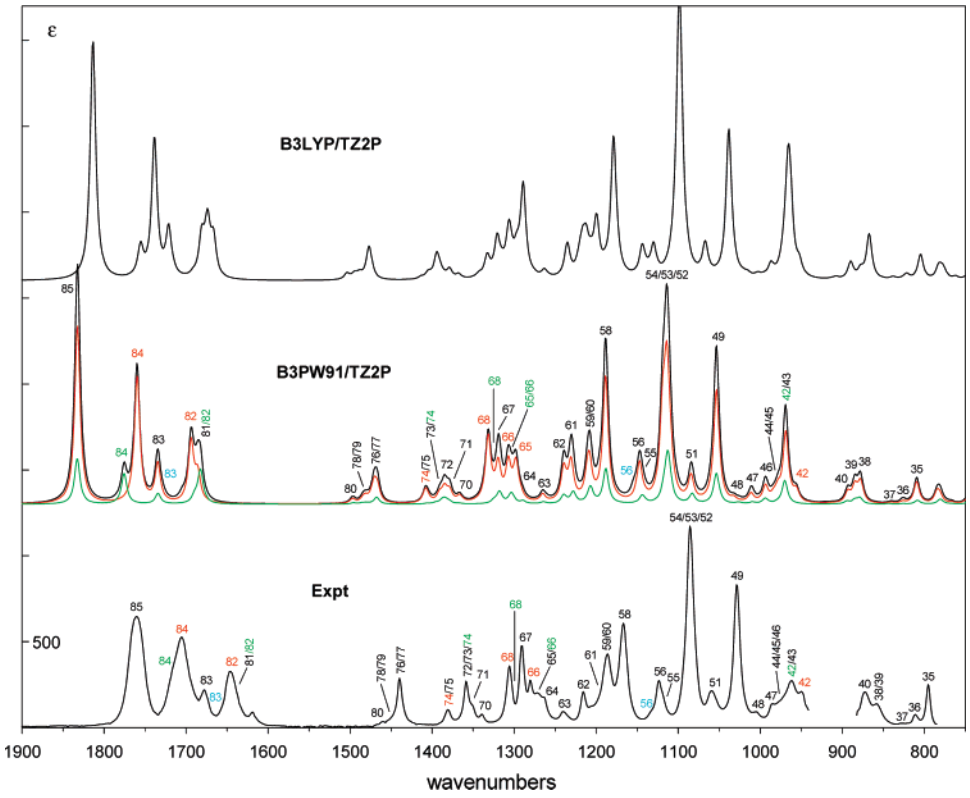

FIGURE 10. Comparison of the experimental and B3LYP/TZ2P and B3PW91/TZ2P IR spectra of **2** for the range of 750−1900 cm^{-1}. The black calculated spectra are conformationally averaged. The red and green calculated spectra are the population-weighted IR spectra of **2a** and **2b**, respectively. The numbers define the fundamentals contributing to resolved bands. Red, green, and cyan numbers refer to fundamentals of **2a**, **2b**, and **2c**/**2d**, respectively. Black numbers are used when the bands of **2a** and **2b** are not resolved. Bandshapes of the calculated spectra are Lorentzian ($\gamma = 4.0$ cm^{-1}). The assignment of the experimental spectrum is based on the B3PW91/TZ2P calculated spectrum.

ously,[20,21] for both **1** and **2**, the VCD spectra of the four conformations differ substantially. As with the IR spectra, the conformationally averaged VCD spectra are dominated by the contributions of conformations **a** and **b**. The B3LYP/TZ2P and B3PW91/TZ2P conformationally averaged VCD spectra are compared to each other and to the experimental VCD spectra in Figures 16 and 17. As with the IR spectra, the B3LYP/TZ2P and B3PW91/TZ2P VCD spectra differ and the B3PW91/TZ2P spectra are in better agreement with experiment. The assignments are therefore based both on the B3PW91/TZ2P assignments of the IR spectra and on the B3PW91/TZ2P calculated VCD spectra, as detailed in Tables S3 and S4 of the SI and Figures 16 and 17. A small number of bands observed experimentally can be assigned to the modes of individual conformations. For **1**, modes 42, 61, 69, and 72 of **1a** are resolved, as are mode 61 of **1b** and mode 56 of **1c**/**1d**. For **2**, modes 48 and 66 of **2a** are resolved, as is mode 56 of **2c**/**2d**. The good agreement of calculated and experimental VCD spectra further supports the reliability of the B3PW91/TZ2P conformational analyses of **1** and **2** and the VCD spectra of their conformations. Experimental rotational strengths have been obtained from the experimental VCD spectra via Lorentzian fitting with the results given in Figures S14 and S15 of the SI and Tables S3 and S4 of the SI. Calculated and experimental rotational strengths, the latter conformationally averaged where unresolved, are compared in Figures 18 and 19.

The agreement of the calculated spectrum of (1*R*,5*S*,8*S*,9*S*,-10*S*)-**1** with the experimental spectrum of (+)-**1** unambiguously shows that the AC of the naturally occurring (+)-**1** is 1*R*,5*S*,8*S*,9*S*,10*S*. In Figure 20, the B3PW91/TZ2P calculated VCD spectra for both ACs, 1*R*,5*S*,8*S*,9*S*,10*S* and 1*S*,5*R*,8*R*,9*R*,-10*R*, are compared to the experimental spectrum of (+)-**1**. The spectrum for the 1*S*,5*R*,8*R*,9*R*,10*R* AC is unambiguously inconsistent with experiment. Similarly, comparison of the calculated rotational strengths for the two ACs to the experimental rotational strengths, shown in Figure 18, clearly demonstrates the superior agreement of the rotational strengths for the 1*R*,5*S*,8*S*,9*S*,10*S* AC. Likewise, as seen from Figures 19 and 21, the AC of the naturally occurring (+)-**2** is also unambiguously 1*R*,5*S*,8*S*,9*S*,10*S*.

Electronic Circular Dichroism (ECD) Spectra. The ECD spectrum of a 0.68 mM acetonitrile solution of (+)-**1** over the range of 190−330 nm was reported by Elsässer et al.[11] and is shown in Figure 22. Three features are observed at 237, 215, and 192 nm, with positive, negative, and positive ECD, respectively. The excitation energies, oscillator strengths, and rotational strengths of the lowest 20 electronic excitations of conformations **1a**−**1d** of (1*R*,5*S*,8*S*,9*S*,10*S*)-**1** have been calculated at the B3LYP/aug-cc-pVDZ//B3LYP/6-31G* level with the results given in Table S5 of the SI. The origin-independent velocity rotational strengths and the excitation wavelengths are plotted in Figure S16 of the SI, together with the ECD spectra obtained thence using Gaussian bandshapes ($\sigma = 0.2$ and 0.4 eV). Equilibrium population weighted ECD spectra are shown in Figure S17 of the SI, together with the sum, the conformationally averaged ECD spectrum. In Figure 22, we compare the calculated conformationally averaged ECD spectra for both enantiomers of **1** to the experimental spectrum. The oscillatory

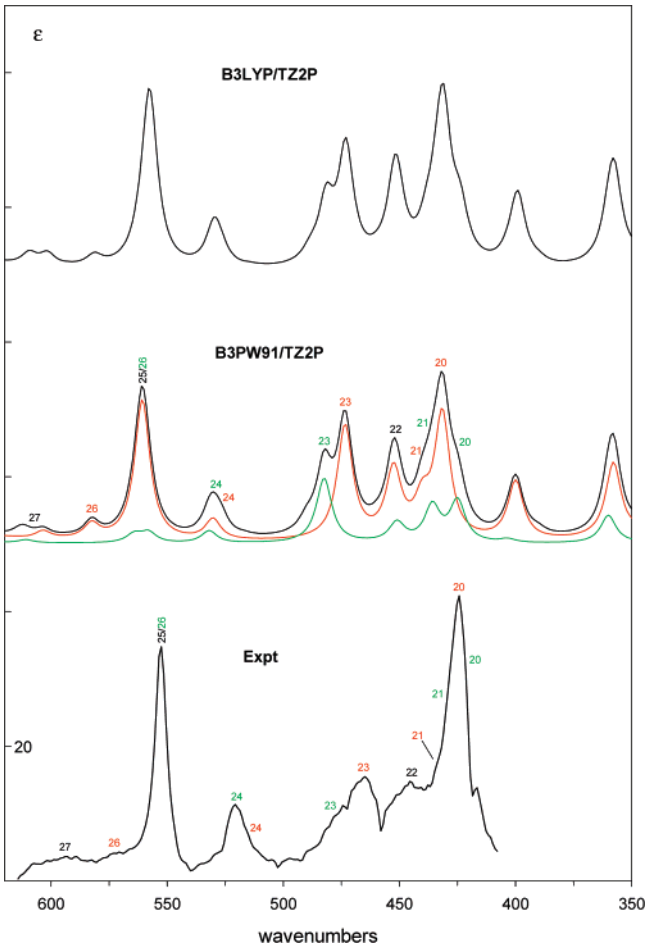

FIGURE 11. Comparison of the experimental and B3LYP/TZ2P and B3PW91/TZ2P IR spectra of **2** for the range of 350−650 cm^{-1}. The black calculated spectra are conformationally averaged. The red and green calculated spectra are the population-weighted IR spectra of **2a** and **2b**, respectively. The numbers define the fundamentals contributing to resolved bands. Red, green, and cyan numbers refer to fundamentals of **2a**, **2b**, and **2c**/**2d**, respectively. Black numbers are used when the bands of **2a** and **2b** are not resolved. Bandshapes of the calculated spectra are Lorentzian (γ = 4.0 cm^{-1}). The assignment of the experimental spectrum is based on the B3PW91/TZ2P calculated spectrum.

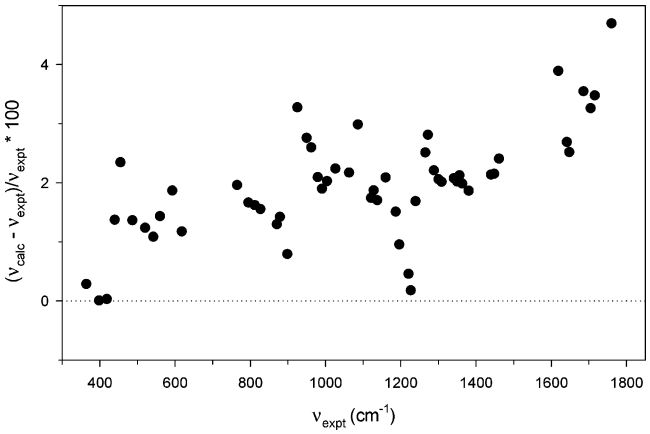

FIGURE 12. Comparison of experimental and B3PW91/TZ2P frequencies of **1**.

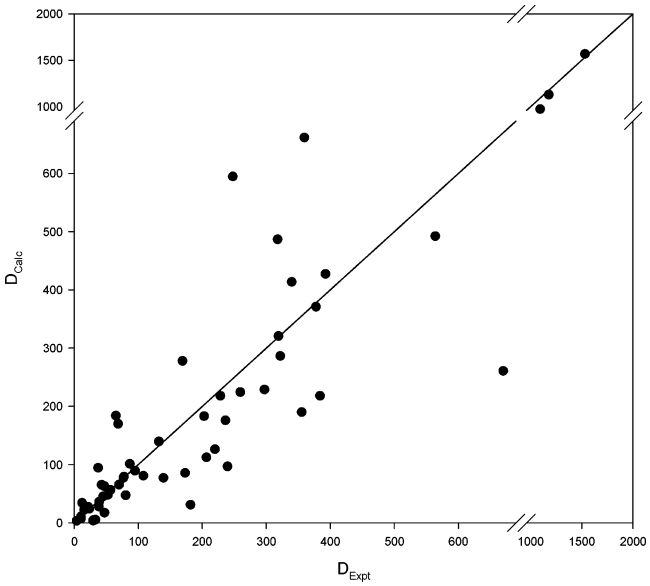

FIGURE 13. Comparison of experimental and B3PW91/TZ2P calculated dipole strengths of **1**. Calculated dipole strengths are population-weighted averages. The line is of +1 slope. Dipole strengths are in 10^{-40} esu^2 cm^2.

character of the ECD spectrum, together with the considerable sensitivity of the predicted spectra to the choice of the Gaussian bandwidth, complicates the assignment of the AC of **1** from its ECD spectrum. For the AC 1*R*,5*S*,8*S*,9*S*,10*S*, the predicted ECD for σ = 0.2 eV exhibits +, −, +, and − features at 269, 250, 227, and 212 nm, while for σ = 0.4 eV, only three features are visible, with −, +, and − signs at 260, 230, and 206 nm. The σ = 0.2 eV spectrum is inconsistent with the experimental spectrum: while the bands at 227 and 212 nm can be assigned to the experimental + and − features at 237 and 215 nm, the predicted − and + bands at 250 and 269 nm are not observed. The agreement of the σ = 0.4 eV spectrum is much better: the bands at 260, 230, and 206 nm can be assigned to the experimental features at 268, 237, and 215 nm. For the AC 1*S*,5*R*,8*R*,9*R*,10*R*, the predicted ECD for σ = 0.2 eV exhibits −, +, −, and + features at 269, 250, 227, and 212 nm, which can be assigned to the experimental bands at 268, 237, 215, and 192 nm. With the σ = 0.4 eV spectrum, the agreement is less good: while the − feature at 230 nm can be assigned to the experimental feature at 215 nm, the + feature at 260 nm is much weaker than the observed band at 237 nm. Alone, the comparison of calculated and experimental ECD spectra does not provide an unambiguous assignment of the AC of **1**. Given the AC established unambiguously by the VCD spectrum of **1**, the correct assignment of the ECD spectrum must in fact be based on the calculated spectrum for (1*R*,5*S*,8*S*,9*S*,10*S*)-**1**. Given the much better agreement of the σ = 0.4 eV spectrum with experiment, we conclude that the −, +, and −, 268, 237, and 215 nm bands of the experimental spectrum are best assigned to the 260, 230, and 206 nm features of the calculated spectrum.

The ECD spectrum of a 0.53 mM acetonitrile solution of (+)-**2** over the range of 190−330 nm was also reported by Elsässer et al.[11] and is shown in Figure 23. While the spectrum is not identical to that of (+)-**1**, the overall form is quite similar. B3LYP/aug-cc-pVDZ//B3LYP/6-31G* calculations for (1*R*,5*S*,8*S*,9*S*,10*S*)-**2** (Figures S18 and S19 and Table S6 of the SI) lead to the conformationally averaged ECD spectra of both enanti-

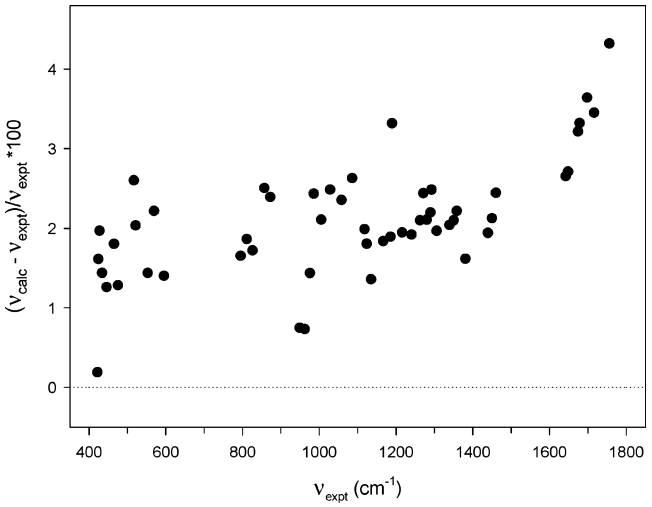

FIGURE 14. Comparison of experimental and B3PW91/TZ2P frequencies of **2**.

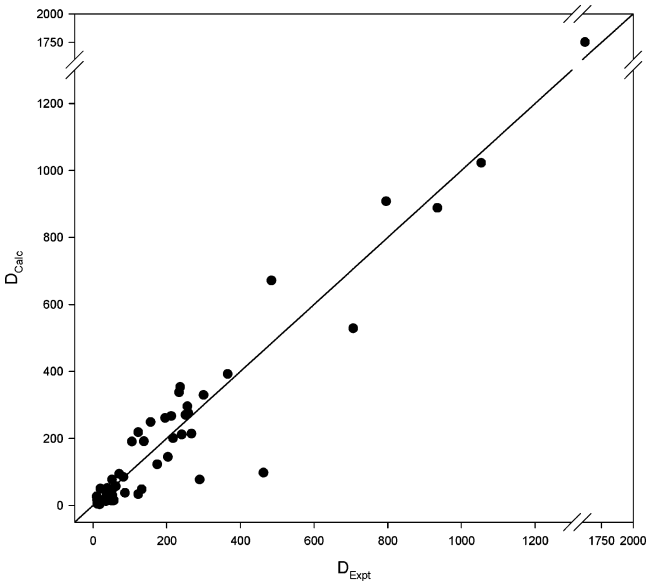

FIGURE 15. Comparison of experimental and B3PW91/TZ2P calculated dipole strengths of **2**. Calculated dipole strengths are population-weighted averages. The line is of +1 slope. Dipole strengths are in 10^{-40} esu^2 cm^2.

omers of **2** shown in Figure 23. The predicted spectra of **2** are very similar to those for **1** (with the same AC). As with **1**, comparison of calculated and experimental ECD spectra of **2** does not provide an unambiguous assignment of the AC of **2**.

Specific Rotations. The specific rotations, $[\alpha]_D$, of **1** and **2** have been reported, with the results given in Tables 3 and 4. The $[\alpha]_D$ values of the samples used for the VCD measurements reported above are +178.2 (*c* 2.01, $CDCl_3$) for (+)-**1** and +214.6 (*c* 0.92, $CDCl_3$) for (+)-**2**, consistent with most literature values (Tables 3 and 4). To date, to the best of our knowledge, no enantiomeric excesses of naturally occurring samples of **1** or **2** have been determined. The agreement of calculated and experimental vibrational rotational strengths for **1** and **2** supports the conclusion that the enantiomeric excesses of the samples of **1** and **2** used in this work are high.

The $[\alpha]_D$ values of the conformations **a**−**d** of (1*R*,5*S*,8*S*,9*S*,-10*S*)-**1** and (1*R*,5*S*,8*S*,9*S*,10*S*)-**2** have been calculated at the

TABLE 3. Experimental and Calculated Optical Rotations of 1[a]

	$[\alpha]_D$	$[\alpha]_{578}$	$[\alpha]_{546}$	$[\alpha]_{436}$
1a	+227.7	+238.3	+272.9	+481.9
1b	+215.5	+225.8	+259.9	+473.0
1c	−51.3	−54.4	−64.8	−141.9
1d	−87.2	−91.9	−107.7	−217.2
avg[b]	+194.9	+204.0	+233.8	+414.5
expt[c]	+178.2[d]	+186.8	+215.3	+389.1

[a] Specific rotations in degrees·[dm·g/cm^3]$^{-1}$. [b] Conformational averages are based on the populations obtained from the B3LYP/6-31G* relative free energies (Table 1). [c] The experimental values are for (+)-**1** in $CDCl_3$ (*c* 2.01). The calculated values are for (1*R*,5*S*,8*S*,9*S*,10*S*)-**1** at the B3LYP/aug-cc-pVDZ//B3LYP/6-31G* level. [d] Reported $[\alpha]_D$ values for **1** are +204 ($CHCl_3$),[2] +197.5 (*c* 0.982, $CHCl_3$),[3b] +86.68,[6] +178.6 (*c* 0.23, $CHCl_3$),[5c] +200 (*c* 0.1, $CHCl_3$),[4a] +173 (*c* 1.10, $CHCl_3$),[5h] +179 (*c* 14.6, $CHCl_3$).[11]

TABLE 4. Experimental and Calculated Optical Rotations of 2[a]

	$[\alpha]_D$	$[\alpha]_{578}$	$[\alpha]_{546}$	$[\alpha]_{436}$	$[\alpha]_{365}$
2a	+245.6	+257.1	+294.4	+519.7	+858.8
2b	+228.3	+239.3	+275.3	+499.1	+861.9
2c	0.0	−0.7	−3.4	−34.3	−133.4
2d	−37.8	−40.2	−48.6	−114.0	−267.0
avg[b]	+213.4	+223.4	+255.8	+451.8	+747.2
expt[c]	+214.6[d]	+224.6	+258.5	+473.9	+822.4

[a] Specific rotations in degrees·[dm·g/cm^3]$^{-1}$. [b] Conformational averages are based on the populations obtained from the B3LYP/6-31G* relative free energies (Table 2). [c] The experimental values are for (+)-**2** in $CDCl_3$ (*c* 0.92). The calculated values are for (1*R*,5*S*,8*S*,9*S*,10*S*)-**2** at the B3LYP/aug-cc-pVDZ//B3LYP/6-31G* level. [d] Reported $[\alpha]_D$ values for **2** are +216.4 (*c* 1.01, $CHCl_3$),[3b] +189 (*c* 0.61, $CHCl_3$),[5h] +194 (*c* 0.64, $CHCl_3$).[11]

B3LYP/aug-cc-pVDZ//B3LYP/6-31G* level with the results given in Tables 3 and 4. The conformationally averaged $[\alpha]_D$ values of **1** and **2** are +194.9 and +213.4, respectively, in excellent agreement with our experimental values, the differences being 16.7 and 1.2. For the enantiomers, (1*S*,5*R*,8*R*,9*R*,-10*R*)-**1** and -**2**, the predicted $[\alpha]_D$ values are −194.9 and −213.4, differing from the experimental values by 373.1 and 418.0, respectively. It follows with high certainty that the ACs of (+)-**1** and (+)-**2** are (1*R*,5*S*,8*S*,9*S*,10*S*), identical to the ACs derived from their VCD spectra. Additional confidence in the TDDFT specific rotation calculations is provided by the further comparison of the $[\alpha]$ values at the wavelengths 578, 546, and 436 nm. Experimentally, for both **1** and **2**, $[\alpha]$ increases monotonically with decreasing wavelength. The calculated $[\alpha]$ values increase in parallel. Thus, as shown in Figure 24, the calculated and experimental dispersions of $[\alpha]$ for both **1** and **2** are in excellent agreement, further supporting the reliability of the TDDFT calculations and the ACs of **1** and **2** derived thence.

Discussion

The experimental measurements of the VCD, OR, and ECD of **1** and **2** have been carried out using liquid solutions at room temperature. The calculation of these properties therefore requires initially the conformational analysis of **1** and **2**, i.e. the prediction of the structures and relative energies of the conformations of **1** and **2**, which are significantly populated at room temperature. In this work, we have carried out conformational analysis via the protocol used in previous publications.[20−25] First, Monte Carlo searching using the molecular mechanics force field MMFF94 is carried out with a window of 10 kcal/mol. For both **1** and **2**, this yields four conformations,

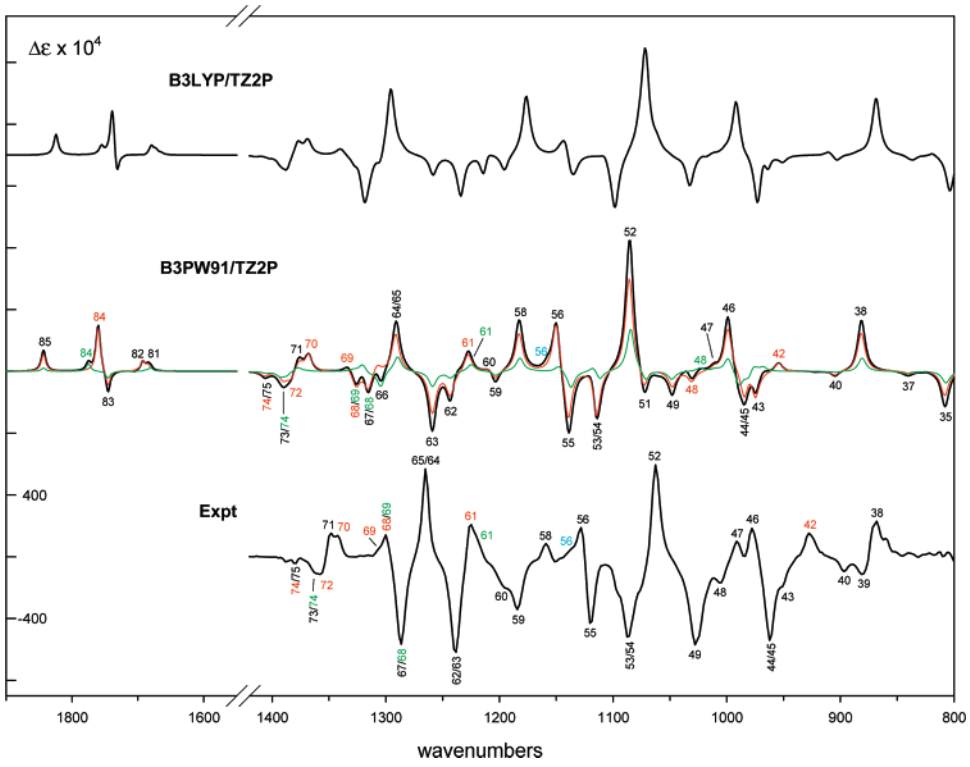

FIGURE 16. Comparison of the experimental and B3LYP/TZ2P and B3PW91/TZ2P VCD spectra of **1** for the range of 800−1900 cm^{-1}. The black calculated spectra are conformationally averaged. The red and green calculated spectra are the population-weighted VCD spectra of **1a** and **1b**, respectively. The numbers define the fundamentals contributing to resolved bands. Red, green, and cyan numbers refer to fundamentals of **1a**, **1b**, and **1c**/**1d**, respectively. Black numbers are used when the bands of **1a** and **1b** are not resolved. Bandshapes of the calculated spectra are Lorentzian ($\gamma = 4.0$ cm^{-1}). The assignment of the experimental spectrum is based on the B3PW91/TZ2P calculated spectrum.

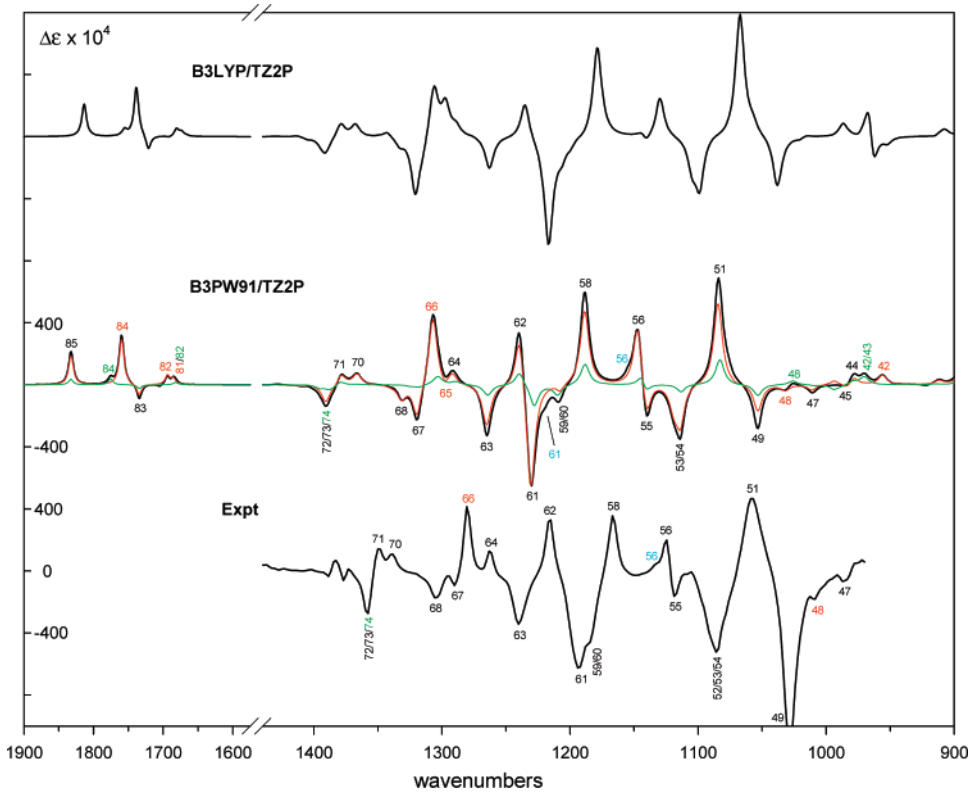

FIGURE 17. Comparison of the experimental and B3LYP/TZ2P and B3PW91/TZ2P VCD spectra of **2** for the range of 900−1900 cm^{-1}. The black calculated spectra are conformationally averaged. The red and green calculated spectra are the population-weighted VCD spectra of **2a** and **2b**, respectively. The numbers define the fundamentals contributing to resolved bands. Red, green, and cyan numbers refer to fundamentals of **2a**, **2b**, and **2c**/**2d**, respectively. Black numbers are used when the bands of **2a** and **2b** are not resolved. Bandshapes of the calculated spectra are Lorentzian ($\gamma = 4.0$ cm^{-1}). The assignment of the experimental spectrum is based on the B3PW91/TZ2P calculated spectrum.

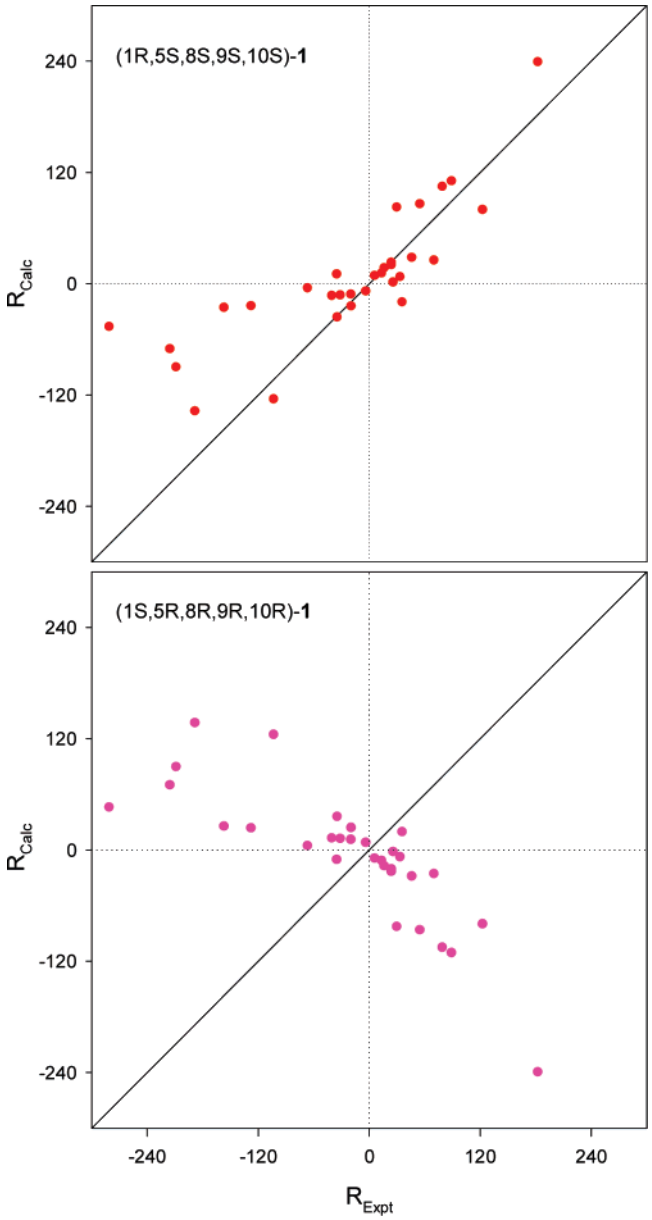

FIGURE 18. Comparison of B3PW91/TZ2P calculated and experimental rotational strengths of **1**. Experimental rotational strengths are for (+)-**1**. Calculated rotational strengths are for (1*R*,5*S*,8*S*,9*S*,10*S*)-**1** (top) and (1*S*,5*R*,8*R*,9*R*,10*R*)-**1** (bottom). Calculated rotational strengths are population-weighted averages. The solid line is of +1 slope. Rotational strengths are in 10^{-44} esu^2 cm^2.

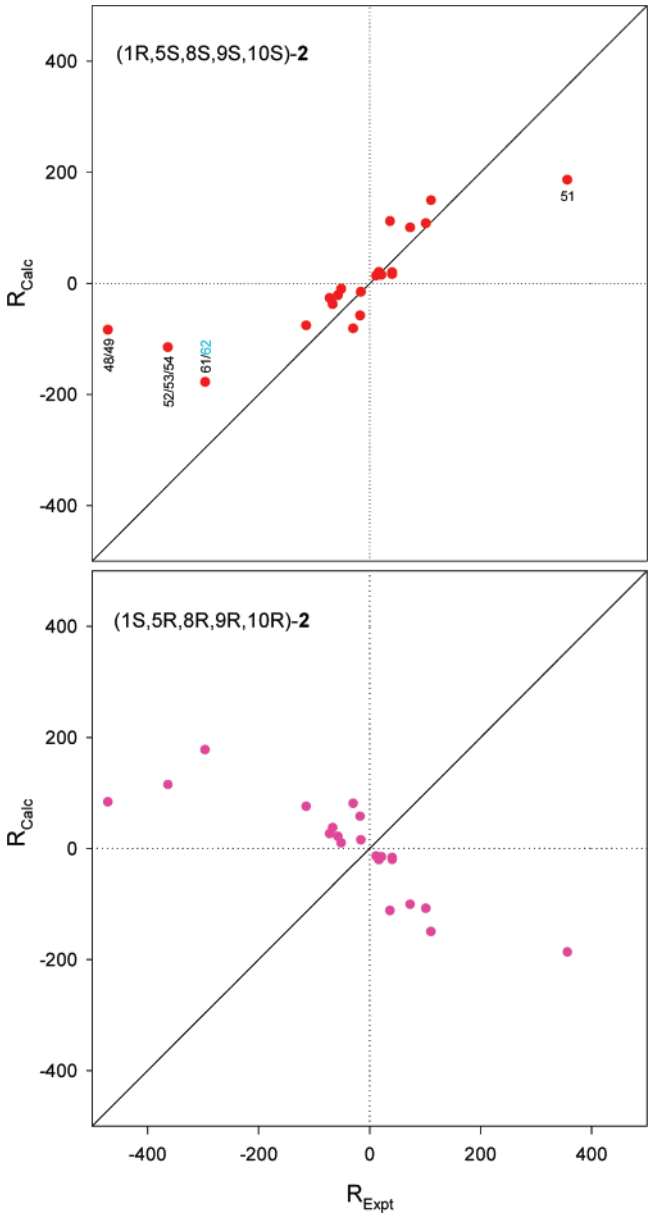

FIGURE 19. Comparison of B3PW91/TZ2P calculated and experimental rotational strengths of **2**. Experimental rotational strengths are for (+)-**2**. Calculated rotational strengths are for (1*R*,5*S*,8*S*,9*S*,10*S*)-**2** (top) and (1*S*,5*R*,8*R*,9*R*,10*R*)-**2** (bottom). Calculated rotational strengths are population-weighted averages. The solid line is of +1 slope. Rotational strengths are in 10^{-44} esu^2 cm^2.

a−**d**, with energies lying within a range of 2 kcal/mol. These initial estimates of the conformational structures and energies of **1** and **2** are then refined by reoptimizations using DFT, initially at the B3LYP/6-31G* level and subsequently at the B3LYP/TZ2P and B3PW91/TZ2P levels. Although in some molecules the MMFF94 and DFT potential energy surfaces (PESs) can differ substantially, leading to very different structures and energies of the stable conformations,[20−25] in the cases of **1** and **2**, the DFT and MMFF94 structures and relative energies are not very different.

The four conformations, **a**−**d**, of **1** and **2** differ principally with regard to the conformations of rings B and D and of the methoxycarbonyl substituent of ring D. As expected, rings B and D are substantially nonplanar. As clearly seen in Figures 1 and 3, in all conformations, these rings are oppositely puckered so that the distance between oxygen atoms O_a and O_b is maximized. In all conformations, rings A and C are close to planar. As to be expected, two conformations of the methoxycarbonyl group are predicted for each conformation of the quadracyclic cores of **1** and **2**, with the C═O group coplanar with and either s-*cis* or s-*trans* to the ethylenic moiety C3═C4. In all conformations, the O═C15−O−C16 acetate moiety is *cis*.

The existence of X-ray structures of **1** and **2** enables the reliability of the MMFF94 and DFT structures to be assessed. As demonstrated in Figures 2 and 5, the agreement of calculated and experimental dihedral angles is excellent for conformations **a** of **1** and **2**, with rms deviations of ∼5 and ∼4° for **1a** and **2a**,

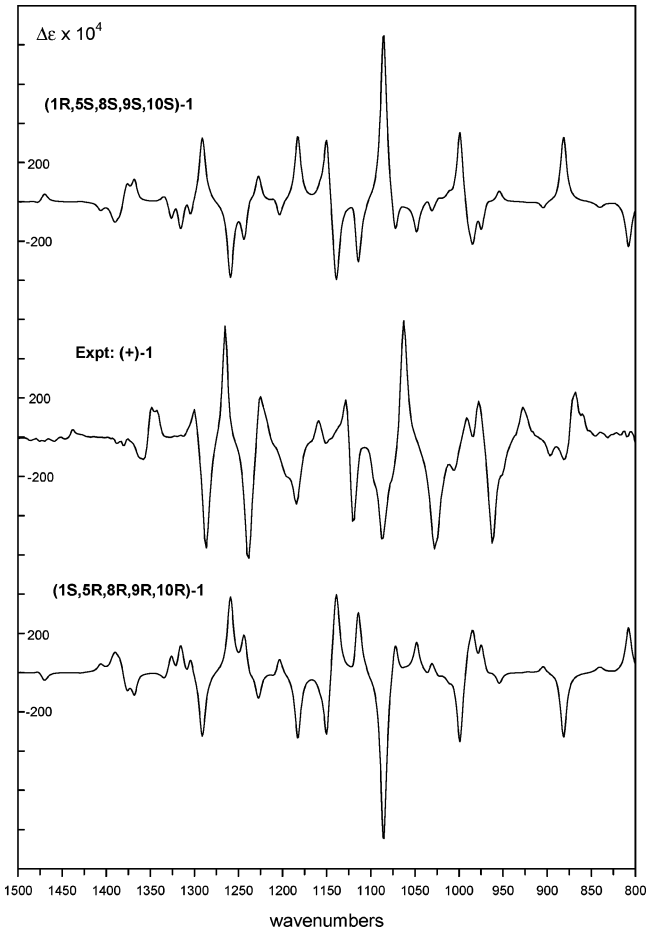

FIGURE 20. Comparison of the experimental VCD spectrum of (+)-**1** and the B3PW91/TZ2P calculated VCD spectra of the two enantiomers of **1**.

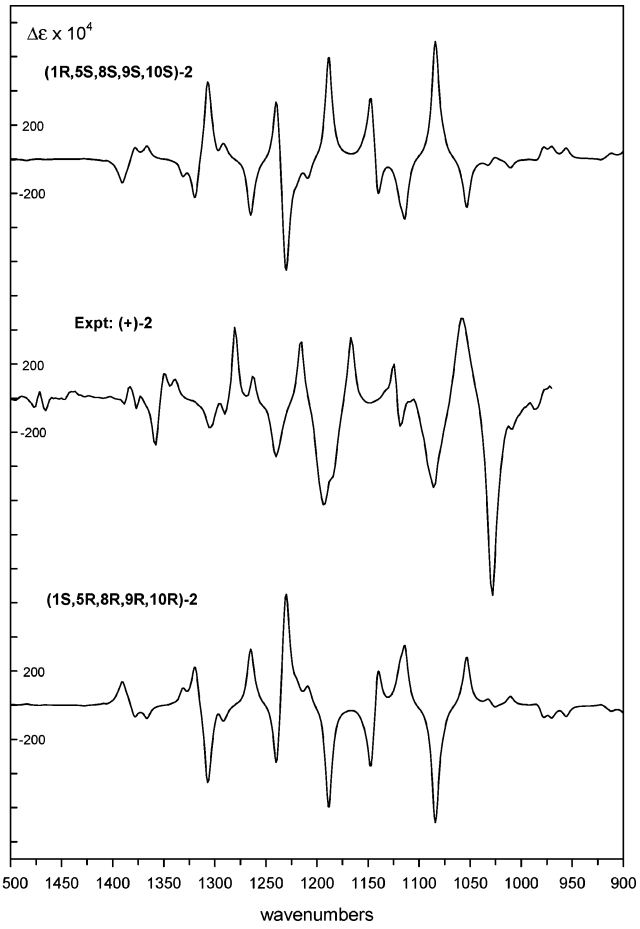

FIGURE 21. Comparison of the experimental VCD spectrum of (+)-**2** and the B3PW91/TZ2P calculated VCD spectra of the two enantiomers of **2**.

respectively, at all calculational levels, and very poor for conformations **b**−**d**. Thus, the conformations of **1** and **2** in the crystalline state are clearly those of the predicted conformations of lowest energy, **1a** and **2a**, and for these conformations, calculated and experimental geometries are in good agreement. Of course, in the absence of experimental geometries for conformations **b**−**d**, we cannot compare calculated and experimental geometries for all predicted conformations, as was possible in the case of a chiral barrelenophane where all three predicted low-energy conformations were present in the X-ray structure.[24f]

In predicting the room-temperature equilibrium populations of conformations **a**−**d** of **1** and **2**, we use the relative free energies, obtained using the DFT harmonic vibrational frequency calculations, and Boltzmann statistics. On this basis, we predict the populations of conformations **c** and **d** to be small: ∼10% at the B3LYP/6-31G* level and ∼5% for **1** and 6−8% for **2** at the B3LYP/TZ2P and B3PW91/TZ2P levels (Tables 1 and 2). It follows that the major contributions to the VCD, OR, and ECD of **1** and **2** are predicted to arise from conformations **a** and **b** alone.

Vibrational spectra are sensitive to the molecular geometry and, therefore, to the conformation. Accurate vibrational spectra of conformationally flexible molecules can therefore be predicted only when the conformational structures and populations are accurately predicted. Comparison of the conformationally averaged IR and VCD spectra of **1** and **2** to the corresponding experimental spectra thus enables the reliability of our conformational analyses of **1** and **2** to be evaluated. As shown in Figures 8−11, the B3PW91/TZ2P IR spectra are in excellent agreement with the experimental IR spectra, permitting detailed assignments of the latter. Most importantly, as discussed in detail above, bands originating in individual conformations alone are resolved, with relative intensities consistent with the intensities predicted using the B3PW91/TZ2P relative free energies. If the experimental conformations were substantially different in number, structures, and relative free energies from our predicted conformations, the predicted IR spectra would be in much poorer agreement with experiment. The quality of the agreement observed strongly supports the reliability of the conformational analyses of **1** and **2**. Of course, the agreement of calculated and experimental IR spectra is not perfect. Quantitative evaluation of the agreement is provided by comparison of the experimental frequencies and dipole strengths obtained via Lorentzian fitting of the IR spectra to the calculated values. As shown in Figures 12 and 14, calculated frequencies are systematically greater than experimental frequencies. As is well-known,[31] the errors in the

(27) Cheng, J. C.; Nafie, L. A.; Stephens, P. J. *J. Opt. Soc. Am.* **1975**, *65*, 1031−1035.
(28) *Spartan 02*; Wavefunction, Inc., www.wavefun.com.
(29) (a) Kawiecki, R. W.; Devlin, F. J.; Stephens, P. J.; Amos, R. D.; Handy, N. C. *Chem. Phys. Lett.* **1988**, *145*, 411−417. (b) Devlin, F. J.; Stephens, P. J.; Cheeseman, J. R.; Frisch, M. J. *J. Phys. Chem. A* **1997**, *101*, 6322−6333. (c) Devlin, F. J.; Stephens, P. J.; Cheeseman, J. R.; Frisch, M. J. *J. Phys. Chem. A* **1997**, *101*, 9912−9924.

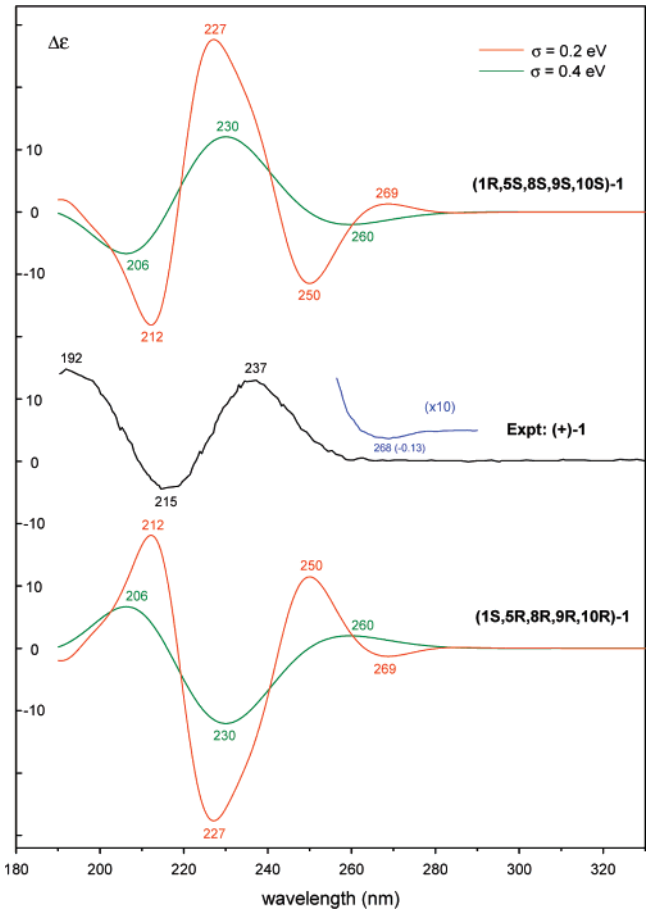

FIGURE 22. Comparison of the experimental ECD spectrum of (+)-**1** and the calculated ECD spectra of the two enantiomers of **1**. Bandshapes of the calculated spectra are Gaussian (σ = 0.2 and 0.4 eV).

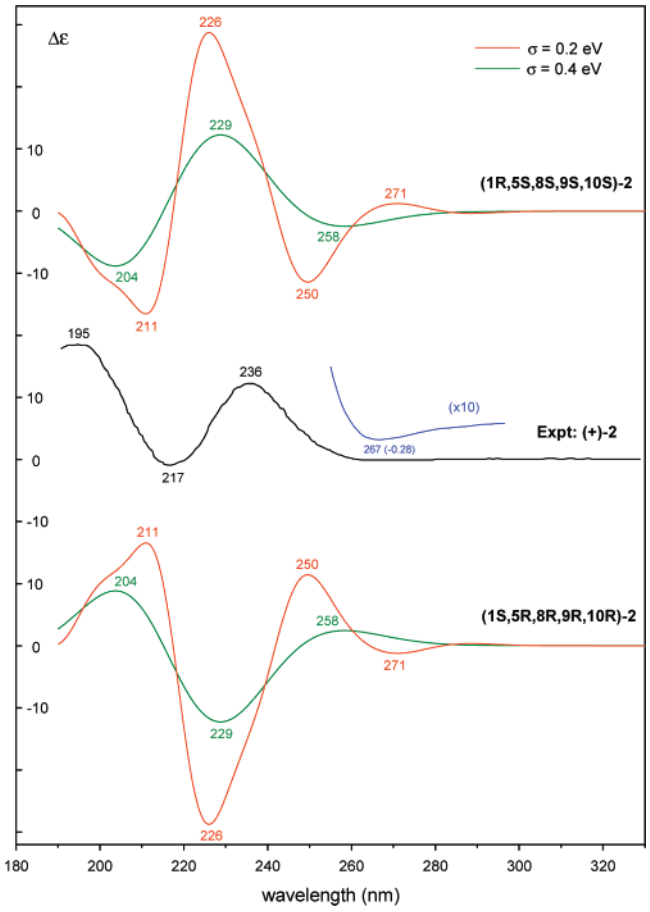

FIGURE 23. Comparison of the experimental ECD spectrum of (+)-**2** and the calculated ECD spectra of the two enantiomers of **2**. Bandshapes of the calculated spectra are Gaussian (σ = 0.2 and 0.4 eV).

calculated frequencies originate predominantly in the neglect of anharmonicity in the vibrational force field. To a lesser extent, errors also arise from the neglect of solvent effects and from the inexactness of the density functional used. In the case of the dipole strengths, the deviations between calculated and experimental values can be attributed not only to the neglect of anharmonicity and solvent effects and the imperfection of the functional but also to the inexactness of the calculated conformational relative free energies and equilibrium populations.

The assignments of the IR spectra of **1** and **2** lead automatically to the assignments of the VCD spectra since every vibrational transition contributing to the VCD spectrum occurs at a frequency identical to that of the corresponding transition in the IR spectrum. Comparison of the experimental VCD spectra of (+)-**1** and (+)-**2** to the predicted VCD spectra for the two enantiomers of **1** and **2** then leads to the ACs of (+)-**1** and (+)-**2**. As shown in Figures 16 and 17, with very few exceptions, the signs of the VCD intensities for (1*R*,5*S*,8*S*,9*S*,-10*S*)-**1** and -**2** are in agreement with the experimental signs for the corresponding transitions. For the same transitions, the signs for (1*S*,5*R*,8*R*,9*R*,10*R*)-**1** and -**2** are in disagreement. It follows that the ACs of **1** and **2** must be (1*R*,5*S*,8*S*,9*S*,10*S*)-(+). Lorentzian fitting of the experimental VCD spectrum gives the experimental rotational strengths of the observed transitions of (+)-**1** and (+)-**2**. Comparison to the calculated rotational strengths for the two enantiomers of **1** and **2**, shown in Figures 18 and 19, clearly confirms the superior agreement for the 1*R*,5*S*,8*S*,9*S*,10*S* enantiomers. As with the dipole strengths, and for the same reasons, quantitative agreement of calculated and experimental rotational strengths is not perfect. However, the errors are very much larger for the 1*S*,5*R*,8*R*,9*R*,10*R* enantiomers, eliminating any possibility that this is the AC of (+)-**1** and (+)-**2**.

Unfortunately, comparison of the TDDFT ECD spectra of the two enantiomers of **1** and **2** to the experimental ECD spectra of (+)-**1** and (+)-**2** does not lead to a definitive assignment of the ACs of **1** and **2**. The high densities of electronic transitions predicted over the range of 190−280 nm and the bisignate nature of their rotational strengths lead to ECD spectra which oscillate in sign, with maxima and minima which vary in wavelength and intensity with the bandwidth parameter, σ. As a result, assignment of the peaks and troughs observed in the experimental ECD spectra are not unambiguous.

The use of transparent spectral region optical rotations at a small number of wavelengths to determine ACs is procedurally much simpler than the use of VCD and ECD spectra. All that needs to be done is to compare the signs and magnitudes of predicted and experimental specific rotations at each wavelength and the shapes of the predicted and experimental dispersions (wavelength dependences). As seen in Figure 24, for (+)-**1** and (+)-**2**, the predicted specific rotations from 589 to 436 nm for (1*R*,5*S*,8*S*,9*S*,10*S*)-**1** and -**2** are in excellent agreement with

(30) *PeakFit*, 4th ed.; Jandel Scientific Software, 1995.
(31) Finley, J. W.; Stephens, P. J. *J. Mol. Struct. (THEOCHEM)* **1995**, *357*, 225−235.

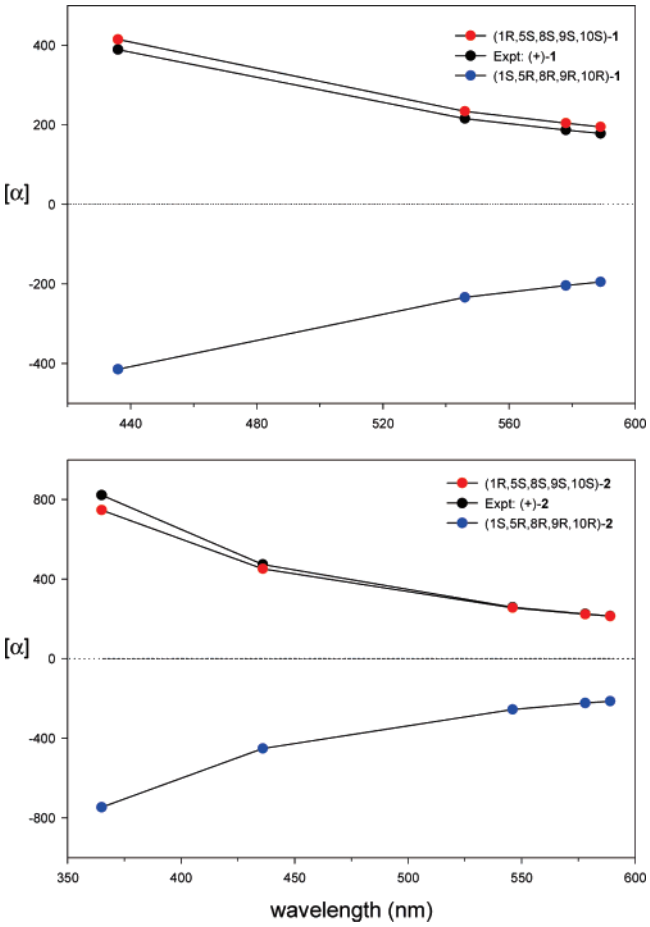

FIGURE 24. Comparison of experimental and calculated $[\alpha]_\lambda$ of **1** and **2**.

experiment, in contrast to those predicted for the 1*S*,5*R*,8*R*,9*R*,-10*R* AC, providing further support for the (1*R*,5*S*,8*S*,9*S*,10*S*)-(+) ACs of **1** and **2** deduced from their VCD spectra.

Thus, in the cases of **1** and **2**, it turns out that the VCD and OR yield unambiguous and consistent assignments of their ACs, while the ECD spectra cannot be unambiguously analyzed. The ACs obtained for the naturally occurring (+)-**1** and (+)-**2** are 1*R*,5*S*,8*S*,9*S*,10*S*, identical to those reported by Albers-Schönberg and Schmid.[3] The reversal of these ACs proposed by Elsässer et al.,[11] on the basis of semiempirical calculations of the ECD spectra, is shown to be incorrect.

The AC of plumericin was reported in 1961[3b] by chemical correlation to plumieride whose AC was in turn determined by degradation to (+)-ethylsuccinic acid.[32] Thereafter, plumericin and plumieride served as reference compounds for the structure elucidation of plumeria and allamanda type iridoids and their glycosides[4a,5b,c,26,33,34] since they could be chemically correlated with plumericin or plumieride following the proposed biosynthetic pathway.[9c] The confirmation of the AC of plumericin shows that the ACs of iridoids chemically correlated with plumericin are not in need of change.

Methods

Spectroscopy. IR and VCD spectra of $CDCl_3$ and $CHCl_3$ solutions of (+)-**1** and (+)-**2** were obtained using a Thermo-Nicolet Nexus 670 IR spectrometer and a Bomem/BioTools chiral/IR VCD spectrometer at resolutions of 1 and 4 cm^{-1}, respectively. The VCD instrument is equipped with a dual photo-elastic modulator accessory, in order to reduce VCD artifacts, a methodology invented and implemented by Dr. J. C. Cheng at USC in 1975.[27] Harrick cells with KBr windows and 597, 239, and 109 μm pathlengths were used. VCD scan times were 1 h.

Optical rotations were measured using a Perkin-Elmer 241 polarimeter at 25 °C.

Calculations. All calculations have been carried out on (1*R*,5*S*,8*S*,9*S*,10*S*)-**1** and (1*R*,5*S*,8*S*,9*S*,10*S*)-**2**. Initial conformational analysis of **1** and **2** was carried out using Monte Carlo searching together with the MMFF94 force field, via the SPARTAN 02 program.[28] Geometry optimizations of the MMFF94 conformations obtained were then carried out using DFT via the GAUSSIAN 03 program,[19] followed by calculations of their harmonic vibrational frequencies to verify their stability and thence calculations of room-temperature free energies. Simultaneously with vibrational frequency calculations, harmonic vibrational dipole strengths and rotational strengths were also calculated and IR and VCD spectra obtained thence, using Lorentzian bandshapes.[29] The DFT calculations of vibrational rotational strengths in GAUSSIAN 03 use the equation of Stephens[17] and its DFT implementation by Cheeseman et al.,[18] using gauge-invariant atomic orbitals (GIAOs), which guarantee origin-independent rotational strengths.

Experimental vibrational frequencies, dipole strengths, and rotational strengths were obtained from experimental IR and VCD spectra by Lorentzian fitting[29] using the PeakFit program.[30]

Electronic excitation energies, oscillator strengths, and rotational strengths (in both length and velocity representations) of the DFT conformations of **1** and **2** have been calculated using TDDFT via GAUSSIAN 03 and ECD spectra obtained thence using Gaussian bandshapes.[23b]

Optical rotations of the DFT conformations of **1** and **2** have been calculated using TDDFT via GAUSSIAN 03, using the length representation together with GIAOs, giving origin-independent rotations.

As in prior work,[20,21,25] DFT calculations of conformational structures, energies and free energies and vibrational frequencies, dipole strengths, and rotational strengths have used the functionals B3LYP and B3PW91 and the basis sets 6-31G* and TZ2P. TDDFT calculations of electronic excitation energies, oscillator strengths, and rotational strengths and optical rotations have used the functional B3LYP and the basis set aug-cc-pVDZ.[22−25]

Acknowledgment. We are grateful for financial support from the National Science Foundation (to P.J.S., Grants CHE-0209957 and CHE-0614577). We also thank the USC High Performance Computing and Communication (HPCC) facility for computer time, Hewlett-Packard Inc. for the use of an Alpha Server SC (ES45) HP computer, and Dr. J. R. Cheeseman of Gaussian Inc. for his continual assistance and advice. T.K. thanks the Hungarian Scientific Research Fund (OTKA, F-043536) for financial support.

Supporting Information Available: PES scans; dihedral angles of calculated geometries; experimental and calculated IR and VCD spectra and vibrational frequencies, dipole strengths and rotational strengths; Lorentzian fits of IR and VCD spectra; calculated electronic excitation energies, oscillator strengths, rotational strengths, and ECD spectra. This material is available free of charge via the Internet at http://pubs.acs.org.

JO070155Q

(32) Halpern, O.; Schmid, H. *Helv. Chim. Acta* **1958**, *41*, 1109−1154.
(33) Abe, F.; Mori, T.; Yamauchi, T. *Chem. Pharm. Bull.* **1984**, *32*, 2947−2956.
(34) Abe, F.; Chen, R.; Yamauchi, T. *Chem. Pharm. Bull.* **1988**, *36*, 2784−2789.